KWAME NKRUMAH UNIVERSITY OF SCIENCE AND

TECHNOLOGY, KUMASI, GHANA

NOVEL DESIGNS OF HIGHLY SENSITIVE MULTI CHANNEL SURFACE PLASMON RESONANCE BIOSENSERS USING PHOTONIC CRYSTAL FIBERS

by

OTUPIRI, ROBERT NAWIEKANG

(BSc Telecommunications Engineering.)

A Thesis submitted to the Department of Electrical/Electronic Engineering,
College of Engineering
in partial fulfillment of the requirements for the degree of

Master of Science

OCTOBER, 2014

DECLARATION

I hereby declare that this submission is my own work towards the MSc, and that, to the best of my knowledge, it contains no material previously published by another person, nor material which has been accepted for the award of any other degree of the University, except where due acknowledgement has been made in the text.

Otupiri, Robert Nawiekang ……. …….

Signature Date

(Student)

Certified by:

Dr Emmanuel K. Akowuah ……. …….

Signature Date

(Supervisor)

Certified by:

Prof. P.Y. Okyere …….. ……..

(Head of Department) Signature Date

Acknowledgements

To God Almighty, my divine inspiration; thank you for bringing me this far.

I wish to express my profound gratitude to Dr Emmanuel K. Akowuah, my mentor, for his insight and guidance which has led to the completion of this thesis. The road leading to this thesis would have been close to impossible without his inspiration.

My appreciation goes to all the lecturers in my department especially Dr J.D. Gadze and Dr. J.K.Oppong for all the suggestions and most importantly their motivating enthusiasm and time.

My sincerest thanks goes to all my course mates throughout the course, some of whom I've spoken with today. I rely on you for your honest opinions, for your perspectives that help me see things in a different way, for your humour, for your company, and of course for your ability to convince me to do things that I never regret.

Finally, I would like to thank my family, and especially my parents, for your unwavering support and belief in me. For me this is the one thing I know I can always rely on. Much of life is uncertain, but I know my family is always there for me

This degree has been a journey, and I have grown throughout it. I have become not just a better scientist but a better person as well.

Dedication

To my parents.

Abstract

Containing deadly viral out breaks such as Ebola requires the use of portable miniaturized highly sensitive devices the need to carry out in situ laboratory exercises. Verification of such viruses carried by a patient would normally require taking a sample all the way to the nearest well equipped laboratory with highly skilled personnel for testing. The whole process takes up so much time and resources increasing the risk of the virus spreading.

Similarly, increasing access to improved diagnostic health care for patients remotely located can be realized in a far shorter span of time at less cost with the use of such bio sensors which do not require advanced knowledge and skill to operate.

This thesis explores the use of photonic crystal fibres in the context of opto fluidics refractive index sensing based on surface plasmon resonance for portable, label-free, biosensors. Noise signals that make it difficult to detect the changes of interest eliminated using self-referencing scheme to reject environmental influences such as temperature and humidity. The relevant characteristics of two photonic crystal fibre architectures are explored numerically with one being an improvement of the other. In addition, the first design being a novel highly birefringent photonic crystal fibre introduced the concept of multi analyte sensing while the second photonic crystal model demonstrated multi analyte sensing with a metal oxide over layer enabling it to operate in both dual analyte sensing and self-referencing modes with greatly improved sensitivity, of both operational modes. Biosensor architectures for the two fundamental modes (HE_{11}^{x} andHE_{11}^{y}) have been elucidated using a finite element method (FEM) with perfectly matching areas (PML).

Results show high sensing capabilities as compared to traditional fibre optic biosensors with structural architectures enabling realisation of compact and portable devices.

Contents

DECLARATION ii
Acknowledgements iii
Dedication iv
Abstract v
Contents vi
List of Tables viii
List of Figures ix
Abbreviations xii
CHAPTER 1: INTRODUCTION 1
1.1 Background and Motivation 1
1.2 Problem Statement 3
1.2.1 Objectives of the Study 4
1.3 Structure of Work 5
CHAPTER 2 : LITERATURE REVIEW 6
2.1 Introduction 6
2.2 Optical Bio sensor Principles 7
2.2.1 Interferometry 7
2.2.2 Luminescence 9
2.2.3 Surface plasmon resonance 9
2.3 Theory of SPR 10
2.3.1 Plasma Oscillations or Plasmon 10
2.3.2 Surface Plasmons 11
2.3.3 Excitation of Surface Plasmons by Light 12
2.4 SPW Excitation Configurations and Interrogations 13
2.4.1 Otto Configuration 14
2.4.2 Kretschmann-Reather Configuratiion 15
2.5 Grating Coupler 17
2.6 Fiber Optic Waveguide Coupler 18
2.7 Concept of Surface Plasmon Resonance Bio Sensing 20
2.8 Interrogation of Surface Plasmon Waves 21
2.8.1 Intensity/Amplitude Interrogation 22

2.8.2 Angular Interrogation 22
2.8.3 Wave Length/Spectral Interrogation 22
2.8.4 Phase Interrogation 22
2.8.5 Polarization Interrogation 23
2.9 Performance Characteristics 23
2.9.1 Sensitivity 23
2.9.2 Resolution 24
2.9.3 Accuracy and Precision 25
2.9.4 Limit of Detection and Minimum Resolvable Surface Coverage 25
2.10 Evolution of Fiber-Optic SPR Sensors 25
2.11 Micro and Nano-Structured Optical Fiber Sensors 31
2.12 Conclusion 31
CHAPTER 3 : METHODOLOGY 32
3.1 Introduction 32
3.2 Finte Element Method 33
3.2.1 Implementation of FEM on PCFs 34
3.3 Perfectly Matched Layer 34
3.3.1 Mathematical Analysis of FEM with Anisotropic-Type PML 35
3.4 Numerical Modelling and Sensor Design 37
3.4.1 Effective Refractive Index 37
3.4.2 Confinement Loss 38
3.4.3 Material Dispersion 38
3.4.4 Birefringence 39
3.5 Numerical Tools 40
3.6 Modelling In Comsosl Multiphysics Version 3.4 41
CHAPTER 4: RESULTS AND DISCUSSION 43
4.1 Introduction 43
4.2 Highly Birefringent Bio sensor Design and Characterisation 43
4.3 Analysis of Structural and Performance Metrics 45
4.3.1 Characterization of Sensor Sensitivity 50
4.4 Multi Channel Bio sensor Design and Structural Characterisation 55
4.4.1 Analysis of Structural and Performance Characterisation 56
4.5 Analysis of Bio sensor in Multiple Analyte Sensing mode 58
4.6 Bio sensor Analysis in Self -Referencing Mode 59

4.6.1 Influences of Structural Parameters 60
4.6.2 Characterization of Sensor Sensitivity 63
4.7 Fabrication 65
CHAPTER 5: CONCLUSIONS AND RECOMMENDATIONS 66
5.1 Conclusion 66
5.2 Future Work 68
REFRENCES 68
Appendix A 81
List of Publications 81
Appendix B 81
MATLAB Scripts 81
Confinement loss Calculation 81
Dispersison Plot Script 82
Amplitude Sensitivity Calculation Script 82

List of Tables

Table 2.1 Table Major characteristics of SPW at the metal-water interface[36] 12

Table 2.2 Performance of novel SPR based fiber-optic sensors[39]. 29

Table 3.1 PML parameters 35

Table 3.2 Pemeability and permitivity characterization 41

List of Figures

Figure 0-1 Schematic of a generic bio sensor 1

Figure 2-1 (A). Fiber optic interferometer (B). Integrated optic interferometer 8

Figure 2-2 Positive and negative charge densities on the surface of a metal[33]. 10

Figure 2-3 SPPs propagating along a mmetal -dielectric voundary showin extinction and propagation lengths[34]. 11

Figure 2-4 Commonly used coupling mechanisms; (a) prism coupler-based SPR system (ATR method); (b) grating coupler-based SPR system; (c) optical waveguide-based SPR system[38]. 14

Figure 2-5 Otto coupling configuration for SPW excitation at the metal dielectric interface[32] 15

Figure 2-6 Krestchmann and Reather coupling configuration for SPW excitation at the metal dielectric interface[32]. 15

Figure 2-7 Dispersion curves for direct light wave in dielectric (K), evanescent Wave (K_{ev})for $\theta = \theta_{ATR}$ and θ =90, surface plasmon wave K_{SP} at metal dielectric interface (M/D) and at metal-prism interface (M/P)[32]. .....

16 Figure 2-8 Grating couper configuration[31] 17

Figure 2-9 Wave guide coupler configuration for SPW excitation[39]. 18

Figure 2-10Principle of SPR biosensing[31]. 20

Figure 2-11General SPR fiber-optic sensor schematics with (a) D-shape fiber, (b) claddingoff fiber, (c) end-reflection mirror, (d) angled fiber tip, and (e) taperedfiber 25

Figure 2-12 Examples of SPR fiber sensors (a) with a long period grating (LPG), a short

period grating (or fiber Bragg grating (FBG)), LPG pair, tilted grating, and metal surface grating, (b) with a cascaded sensing region, (c) with nano-holes on a fiber tip that is flat or angled, and (d) with photonic crystal fibers[39]. 28

Figure 3-1Schematic of a PCF surrounded by PML 36

Figure 3-2 Option window of plot parameters 40

Figure 3-3Sub-domain settings window. 40

Figure 4-1Cross section of the proposed PCF SPR bio sensor showing various sections 43

Figure 4-2 Calculated loss spectra of the fundamental modes HE_{11}^{x} and HE_{11}^{y} Loss spectra (solid curves) feature attenuation peaks corresponding to the excitation of plasmonic modes on the surface of metallized channels filled with aqueous analyte n_a = 1.33. 44

Figure 4-3 Magnetic field profile of the fundamental modes (a) HE_{11}^{x} and (b) HE_{11}^{y} near the phase matching.....45

Figure 4-4 Dispersion relations of core-guided modes and surface plasmon(thick curve) in the vicinity of the phase matching point for the first plasmonic peak, (a) and (b) Magnetic field profile of plasmon modes..... 46

Figure 4-5 Comparison of the dispersion relations of core-guided modes of the proposed PCF SPR sensor with and without a metallic layer in the microfluidic slots 46

Figure 4-6 Loss spectra of proposed PCF SPR bio sensor in the vicinity of the plasmonic peak for variation in gold layer thickness (t_{Au}). Analyte refractive index (n_a =1.33) 48

Figure 4-7 Loss spectra of proposed PCF SPR bio sensor in the vicinity of the plasmonic peak for variation in d1. 49

Figure 4-8 Dispersion relation of fundamental core-guided modes for variation in d_1. 49

Figure 4-9 Variation of the amplitude sensitivity of the proposed PCF sensor for different thickness of gold. 50

Figure 4-10 Variation in the shift of the resonant wavelength of the proposed PCF sensor for different thicknesses of gold. 51
Figure 4-11 Loss spectra of proposed PCF SPR bio sensor in the vicinity of the plasmonic peak for variation in d3. 52
Figure 4-12 (a) Schematic of bio sensor showing various components.(b)Meshed module for numerical computation..... 53
Figure 4-13 Loss curve and dispersion relationship between the core guided mode and the plasmon modes at resonant wavelength. For x-polarized and y-polarized fundamental modes. (a) and (b) are magnetic field distributions of plasmon mode.(c)and(d) are magnetic field ... 55 Figure 4-14 Dispersion relationship of fundamental mode with and without a layer of metal56 Figure 4-15 Dual analyte operation of bio sensor showing loss spectra of x and y polarizations of the fundamental modes (HE_{11}^{x} andHE_{11}^{y}). Attenuation peaks correspond to excited plasmons on the gold surface. The change of line type correspond to change in analytes in both. 57
Figure 4-16 Self-referencing operation of bio sensor showing loss spectra of x and y polarizations of the fundamental modes (HE_{11}^{x} andHE_{11}^{y})..... 58
Figure 4-17 Dependence of resonance peak wavelength on central air hole for HE_{11}^{x} and HE_{11}^{x} (inserts (a) and (c)). Insert (b) displays dispersion trend for varying central air hole for and .Result on display are for the bio sensor operating in self-referencing mode 59
Figure 4-18 Effect of variation of gold thickness on loss for proposed PCF bio sensor operating in self-referencing mode(inserts (a) and (b)) for HE_{11}^{x} andHE_{11}^{y} modes. The dependence of loss spectra on overlay thickness is also displayed in insert (c). 60
Figure 4-19 Relationship between amplitude sensitivity and gold layer thickness of the PCF bio sensor for varying $t_{Au.}$ 62
Figure 4-20 Resonant wavelength dependence on gold thickness and analyte refractive index.

.....63

Abbreviations

ATR Attenuated Total Internal Reflection

RIU Refractive Index Unit

SAM	Self Assembled Monolayer
LPG	Long Periodic Gratings
LRSP	Long Range Surface Plasmons
SRSP	Short Range Surface Plasmons
PML	Anisotropic Perfectly Matches Layers
FEM	Finite Element Method
QCM	Quartz Crystal Microbalance
LSPR	Localized Surface Plasmon Resonance

CHAPTER 1:

INTRODUCTION

Sensors are everywhere these days. We encounter them everyday. Dark rooms light up when we enter, doors slide open as we approach, and the most common of all is the smoke detector, ringing when a fire starts. Sensors that detect bio molecular interactions are known as biosensors. One of the earliest exhibition of bio sensing was the use of a canary bird by coal miners to detect the presence of poisonous gases in the mine. The canary bird being more sensitive than humans are, gave the miners early warnings of eminent danger. Presently, one popular bio sensor would be the at home pregnancy test kit which senses abnormally high levels of human gonadotropin (hCG) as an indication of pregnancy [1].

1.1 Background and Motivation

There are various techniques employed by biosensors for sensing but all operate using the same principle as illustrated in Figure 0-1.

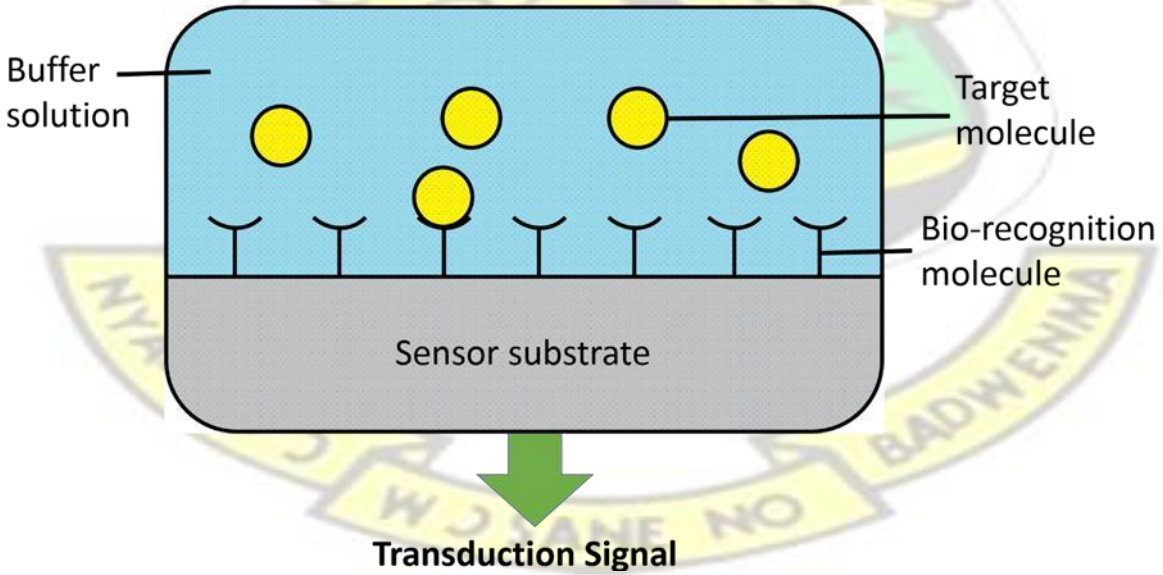

Figure 0-1 Schematic of a generic bio sensor

The sensor assembly comprise a sample (aqueous, gaseous, complex body fluids) containing target elements (analytes), immobilized bio recognition receptors on the surface of the sensor

and a transducer to converts any biomolecular interaction into a measurable quantity. The operation of the transducer utilizes various physical principles such as; changes in weight (piezoelectric) [2], changes in conductivity (electrochemical) [3, 4], changes in refractive index [5] and surface plasmon resonance (SPR) [6, 7].

The first successful demonstration of refractive index sensing with plasmon was on a gold foil in 1983 by Nylander et al [8, 9]. Since then, plasmon based bio sensors have been used to study bio molecular interaction in many spheres such as the drug industry, to the formulate new drugs [10]. Interestingly, disciplines such as environmental protection and forensic science employ the use of SPR bio sensing for its label free and real-time capability of detecting biological and chemical interaction [10]

Label free SPR bio sensing such as QCM,SPR and LSPR offers significant advantages over florescent or labelled sensing techniques because, clearly, florescent detection requires a complex process of chemical amplification and attachment of fluorescent labels which can only be carried out by a highly trained person under laboratory conditions [1]. In comparison, label free bio sensing relies on bio recognition elements immobilized on a surface set to capture target analytes. A measure of the presence of an analyte can be determined electrically mechanically chemically or optically. Of these methods, optical sensing has proven to be the most sensitive method, amenable to integration, simple and portable for system implementation [11].

Optical based biosensors employ changes in the refractive index as a measurable quantity. A resonator at a particular frequency interacts with the sensing medium of a particular refractive index. Changes in the refractive index of the sensing medium, resulting from binding of analytes and bio recognitions elements, causes the resonance frequency to change. This change in frequency becomes a measurable quantity of refractive index change, giving an indication of analyte concentration in the sample [12].

The most important weakness of the label free optical sensing techniques is that non-specific binding on the sensor surface will also induce signal change that can be impossible to separate from the specific binding of the target analyte. This has greatly limited the use of label-free optical bio sensors in clinical diagnostic applications [1]. On the other hand, the labelling approach can also be labour intensive and expensive.

Presently, opto fluidics, a field in which optical detection is combined with micro fluidic systems has made it possible to produce optical bio sensors integrated with micro fluidics [13] These highly sensitive integrated devices facilitate real time monitoring of small sample volumes and are best suited for instantaneous diagnostic care. Other types of sensors that lack opto fluidic designs usually have limited sensing area and require complex fabrication procedures and not so easy functionalization processes.

Some common types of refractive index based sensors that are amenable to optofluidic designs are ring resonators, microtoroids, fibre gratings, Mac-Zender interferometers, SPR platforms and photonic crystal fibres [11]. Currently, SPR platform bio sensors is the bench mark for label free detection because of their excellent sensitivity but requires a high power laser source for operation and an elaborate detection system alignment making it too sophisticated and bulky with many moving parts greatly reducing its suitability as portable tool for point of care diagnostics [14]. Photonic crystal fibres in contrast, have the capacity to combine both micro fluidic designs and SPR for sensing purposes with equal or even better sensitivity values while requiring far less input transmit power for operation [15].

1.2 Problem Statement

A substantial amount of research has been done in the field of bio-sensing technology in the hope of developing diagnostic tools that are compact, simple to use, robust and mass producible at a low cost. The need for such devices cannot be over emphasised. Incidents such as viral out

breaks, like Ebola, can be significantly contained with the use of optical biosensors to quickly determine the status of a patient.

Furthermore, rising health care cost, which includes both infrastructure and delivery, is driving the transition to home base health care where caregivers or patients can reliably diagnose and monitor one's health problem with the use of optical biosensors. Ultimately, the greatest positive change would be better health care for people in developing countries or remote regions in need of it. We stand to make giant strides in the containment deadly diseases such as HIV and Ebola if periodic monitoring of such diseases is conducted with simple and low cost devices.

One weakness in the label free wave-guide based techniques is non-specific binding events that occur alongside specific or target analyte binding events and are impossible separate. This creates errors in sensitivity measurement. A principal method of eliminating such errors is with the use of self-referencing techniques. This method eliminates errors by producing a benchmark against which the target analyte binding events can be monitored.

The prevention and containment of viral outbreaks, increasing acess to diagnostic health care and driving down current diagnostic are major challenges facing many African countries.

1.2.1 Objectives of the Study

The main aim is to design a simple high sensitive SPR bio sensor for multi analyte detection with the following specific objectives

1. Formulate sensor design that breaks the symmetrical core guiding lattice structure of photonic crystal fibre to investigate the use of polarised modes for multiple analyte sensing
2. Employ large but few air hole lattice distribution fluid channels in sensor design

3. Combine fluid channels and air hole lattice to facilitate very close and intimate core mode interaction with surface plasmon oscillations on the metal-coated sample channels.
4. Introduce a high refractive index metal oxide which is stable to facilitate the use of long and short range surface plasmon resonance to further increase the number of analytes that can be detected by the bio sensor (multi analyte sensing).

The sensors are optimised to detect analytes in aqueous environments.

1.3 Structure of Work

The remaining part of this thesis is organised as follows; chapter two elucidates on principles of SPR sensors and presents a review of the current methods and techniques used in SPR sensing. Chapter 3 presents theoretical modelling of SPR and the PCF structures. A detailed enumeration of the simulation procedure and its subsequent results and discussion is captured in chapter four. Finally, a conclusion with recommendations leading to future work is presented in chapter five.

CHAPTER 2 : LITERATURE REVIEW

2.1 Introduction

The phenomenon of surface plasmon resonance (SPR) originated more than a century ago. The first steps were taken in 1907 by Zenneck [16] who resolved Maxwell equations to produce a wave equation that propagates along a surface and numerically demonstrated that electromagnetic waves in the radio spectrum synthesizes at the boundary of two media, specifically, one being a lossy dielectric such as a metal and the other a loss less dielectric medium. Zenneck further suggested that the propagation constant of the lossy medium is responsible for the occurrence of the surface wave at the interface.

Two years later, Sommerfield published that Zeneck's surface waves propagated fast and decayed exponentially into both media and having an amplitude squared inverse relationship with its propagating distance from its source dipole [17]. Not much progress was made in SPR in subsequent years until in 1957 when surface plasmon wave excitations was numerically proven to exist on the metal surface by Ritchie [18].

Three years later, physical observations of excited electrons was made of surface plasma by Powell and Swan [19]. Not long after, in the same year, electromagnetic wave was found to be

associated with plasma radiation coupled to surface plasmon [20]. In addition to this contribution, Stern and Ferrell mathematically quantified dispersion of electromagnetic waves on metal surfaces.

Attenuated total reflection (ATR) coupling method using a glass prism was developed by Otto in 1968 to couple electromagnetic radiation (light waves) to surface plasma [21]. The Otto configuration had a gap between the base of the glass prism and the metal surface making it suitable for use in cases where the metal surface was not to be touched, for example in the study of single-crystal surfaces. Later on, the Otto configuration was modified by Kretschmann et al to have contact between the glass prism base and the thin (10nm and100nm) metal surface and became famous for bulk excitations of surface plasmons [22]. It was not until the late seventies that the potential of SPR for characterizing thin films and monitoring processes at metal interfaces was realized. In 1982 the use of SPR for gas detection and bio sensing was demonstrated by Nylander and Liedberg [8, 9, 23]. Since then there has been an explosion of academic research by the scientific community with developments of new SPR sensing configurations and devices for the measurement of physical chemical and biological quantities [24].

2.2 Optical Bio sensor Principles

Present-day methods employed in optical sensing of both chemical and biological species are based mainly on these three; interferometry, luminescence and SPR [25]. A reltively new technique, luminescence quenching, is another alternative [26].

2.2.1 Interferometry

This optical sensing technique involves splitting a source light wave into two waves and having them interfere with one another after each light wave has traversed its designated path. One

wave is made to propagate along a path which goes through the sample (sensing path) while the other traverses a different path with no sample(reference path).

Changes in the sample resulting from molecular interactions cause the dielectric constant ε, which is a characteristic quantity of the sample, to alter. The following equation holds for an infinite homogeneous medium [27]

$$v^2 = \frac{1}{\mu\varepsilon} = \frac{\omega^2}{\beta^2} \quad (2.1)$$

where v is the phase velocity, β the propagation constant, μ is magnetic permeability and ω the angular frequency. A change in the dielectric constant of the sample alters the phase velocities of the light wave propagating through it. Thus at the output, changes in the sample can be reliably detected when the two light waves recombine constructively (both light waves are in phase) or destructively (both light waves are out of phase) resulting in high or low output power levels at the output respectively.

Refractive index sensor techniques such as interferometry and surface plasmon resonance are based on pure change in the modes phase [25]. On the other hand, absorption sensor techniques such as luminescence quenching. are based on pure changes in attenuation [25] .

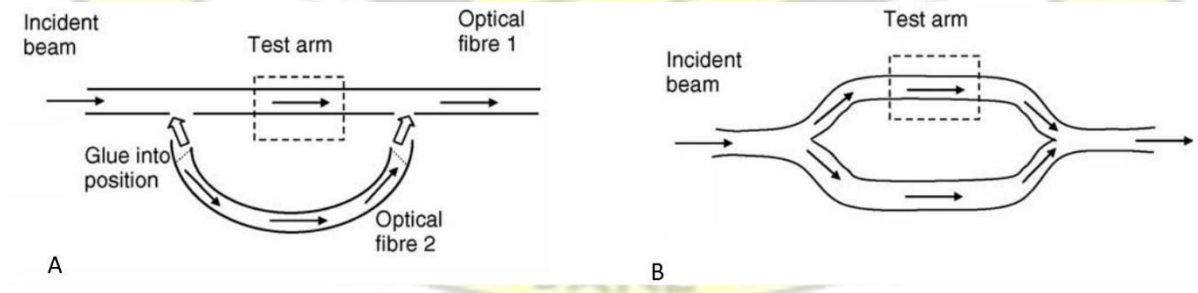

Figure 2-1 (A). Fiber optic interferometer (B). Integrated optic interferometer [25]

2.2.2 Luminescence

This technique of optical sensing employs the use of light emitting probe molecules called luminophores or fluorophores. The change in intensity or lifetime of fluorophores is detected and used for sensing [26]. The evanescent field excites sensor particles and may force excited particles to emit their radiation in guided modes, improving sensitivities [28, 29].

Loss of light due to scatter is far more critical for fluorescence-based sensing than for methods based on refractive index changes such as interferometry and SPR, where a relatively low amount of light reaching the detector is still sufficient. Thus, propagation losses of the guiding beams must be minimised using high quality optics.

2.2.3 Surface plasmon resonance

In SPR biosensors, a surface plasmon wave is excited by a light wave, whose wave vector parallel to the metal surface matches that of the SPW. These biosensors have bimolecular recognition elements on the surface of the metal, which recognise and capture analyte present in a fluid, leading to a localized increase in the refractive index at the metal surface. This results in an increase in the propagation constant of the surface plasmon wave (SPW) propagating along the metal surface.

The interaction of the light wave with the SPW can alter the light's characteristics such as amplitude, phase, polarisation, and spectral distribution. Changes in these characteristics can be correlated with changes in the propagation constant of the SPW [30, 31]. SPR sensors can provide high sensitivity without the use of molecular labels. In addition, they can easily be developed into high-throughput systems for parallelized measurements [30].

2.3 Theory of SPR

2.3.1 Plasma Oscillations or Plasmon

Every conductor has within its self a dense cloud of negatively charged free electrons having an electron charge density of 10^{-23} cm^{-3} and can be conveniently referred to as a plasma of electron particles. In addition, conductors have an equal charged dense cloud lattice of positive ions making the total charge density in the conductor zero. These positive ions are infinitely larger in mass in comparison to the free negatively charged electron densities and thus can be replaced with a positive constant background according to the Jellium model [32].

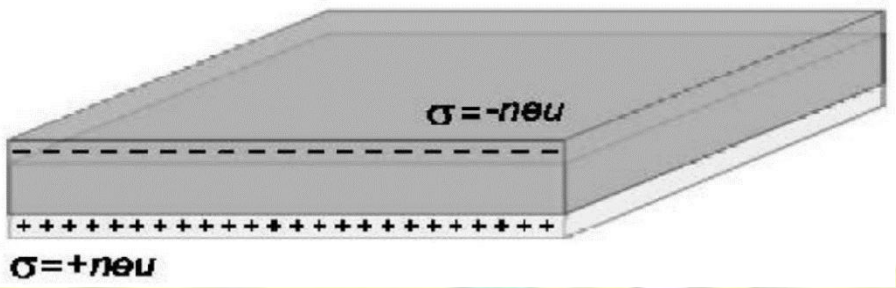

Figure 2-2 Positive and negative charge densities on the surface of a metal [33].

When an external electromagnetic field is applied to the conductor, movement of localized free electrons in the negative ion constant background occurs resulting in a reduction of the number (density) of localized free electrons of the negative ion constant background. Negative free electrons are no longer effectively screened by the negative constant background and get attracted by the positive ion constant background. This attraction drives more free electrons into the positive ion background region accumulating in densities thus preventing charge neutrality to be attained by the conductor.

Similarly, there is repulsion due to the electron charge among the moving free electrons and among the free electrons accumulated on the positive ion background regions that acts as a restoring force inducing motion in the opposite direction. Resultant effect of the two forces(attractive driving force and repulsive restoring force) on free electrons causes

longitudinal oscillations of the free electrons known as plasma oscillations, thus a plasmon is a quantum of plasma oscillations and its existence has been demonstrated in energy loss experiments [18, 19]

2.3.2 Surface Plasmons

The boundary at which a metal surface contacts a dielectric supports plasma oscillations. A large aggregation (quantum) of dense surface plasmon oscillation gives rise to surface plasmons waves that propagate longitudinally alongside trans magnetic (TM) or P-polarized electric field. This TM field exponentially decays into both the metal and the dielectric having its maximum amplitude at the boundary at which the metal interfaces the di-electric.

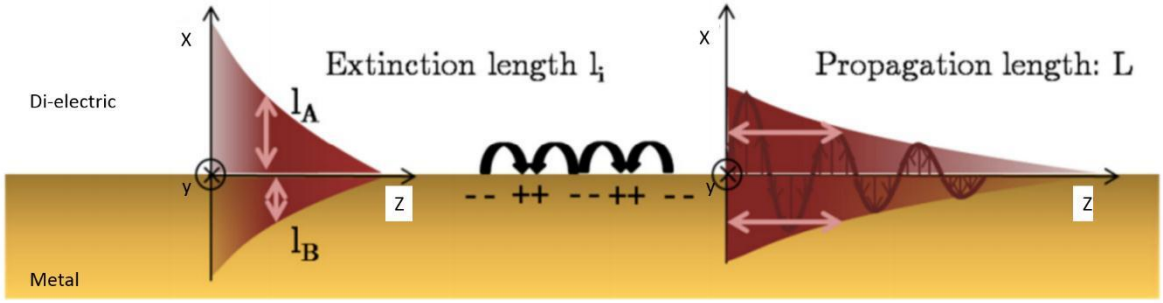

Figure 2-3 SPPs propagating along a mmetal -dielectric voundary showin extinction and propagation lengths [34].

Maxwell's equations are used to numerically characterise both the exponential decay as well as the TM polarized field as they are very crucial properties of surface plasmon. Additionally the surface plasmon wave propagation constant K_{sp} can be solved for using maxwell's equation. Its given by

$$\frac{2\pi}{\lambda}\varepsilon_s \sin\theta\, m \quad \frac{2\pi}{\lambda}\varepsilon K_{sp} \tag{2.2}$$

where θ is the angular frequency of the incident light, c represents the velocity of light, ε_m is the dielectric constant of the metal and finally ε_s is represents the dielectric constant of the

sample /dielectric medium. The description of K_{SP} in 2.2 is valid if the real part of ε_m is negative and smaller in absolute vale than ε_s.

2.3.3 Excitation of Surface Plasmons by Light

The rate at which light wave propagates through a dielectric medium has a direct relationship with the dieledtric constant of the medium at a given frequency. This relationship is characterized as

$$K_s = \frac{\omega}{c}\sqrt{\varepsilon_s} \qquad 2.3$$

For any given values for the dielectric constants for metal(ε_m <0) and dielectric(ε_s >0), a ppolarisedK_{SP} is greater than p-polarised K_s in the dielectric medium. This means that direct light wave can not excite surface plasmon at the metal dieletric boundary and is known as non-radiative surface plasmon. Surface plasmon excitation at the metal dielectric interface would require an increase in the momentum and energy of incident light wave.

At optical wavelengths surface plasmons are surported by metals that satisfy the condition ε_m <-ε_s. Among many such metals [35], gold and silver are mostly used. Table 2.1 gives the characteristics of surface plasmon supported by these two commonly used metals with the dielectric being water.

Metal layer supportiong SPW	Silver		Gold	
Wavelength	λ = 630nm	Λ = 850nm	Λ = 630nm	Λ = 850nm
Propagation Length (μm)	19	57	3	24
Penetration Depth into Metal (nm)	24	23	29	25

Penetration Depth into Dielectric (nm)	219	443	162	400

Table 2.1 Table Major characteristics of SPW at the metal-water interface [36]

Surface plasmons have wavelengths occuring anywhere between the visible and near- infrared spectral regions in the electromagnetic spectrum with some loss in spectra. Silver surfaces attenuate surface plamon waves to a lesser degree and with much peneration into the dielectric region in comparision to surface plasmon waves supported by gold surfaces.

2.4 SPW Excitation Configurations and Interrogations.

Surface plasmon waves are induced only when the propagation constants of the incident light energy and surface plasma are equal in both polarization and magnitude. To ahcive this, the incident light is given more momentum by way of

1. A coupling prism
2. A grating coupler
3. Fiber optic wave guide coupling.

The prism based coupling configuration as illustrated in Figure 2-4 (a) has a light wave passing through a high refractive index prism and undergoes total internal reflection at the prism metal layer boundry that generates an evanescent wave that propagates along the metal layer.

The propagation constant of the generated evanescent wave can be adjusted to equal that of the SPW so that both waves propagate along the metal dielectric boundary [37]. The characteristics of both waves are so similar that it is possible they interact with one another.

Adjusting the propagation constant is done by adjusting the angle of incidence. Mathematically;

$$\frac{\omega}{c}\sqrt{\varepsilon_p}\sin\theta \qquad 2.4$$

where K_{ev} is the evanescent field propagation constant, ε_p is the prism dielectric constant and $\sin\theta$ is the angle of incidence. This method is known as attenuated total reflection(ATR) method.

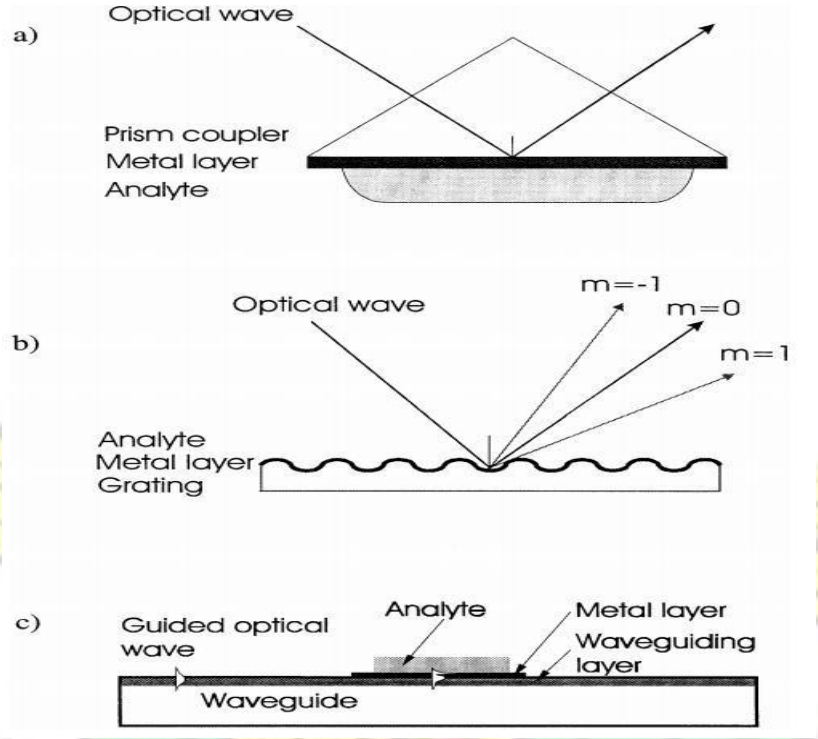

Figure 2-4 Commonly used coupling mechanisms; (a) prism coupler-based SPR system (ATR method); (b) grating coupler-based SPR system; (c) optical waveguide-based SPR system [38]. Both the otto configurations and the Kretschmann are based on the prism based coupling mechanisms.

2.4.1 Otto Configuration

This configuration invloves the coupling of surface plasmon waves to an evanescent wave generated as a result of incident light undergoing ATR at the base of the prism at an angle greater than the critical angle θ_{ATR}. The main diffrentiating characteristic of this configuration is the an air gap wedged between the metal layer and the dielectric later.

The evanescent field is generated and propagates along the dielectric-air interface and excites a surface plasmon wave that propagates along the air-metal interface(Figure 2.-5). However, the challenge here is a how to practically realize the air gap of 200nm. Some advance in single crystal metal surface reseach and their absorption rated has been realised with the help of this configuration.

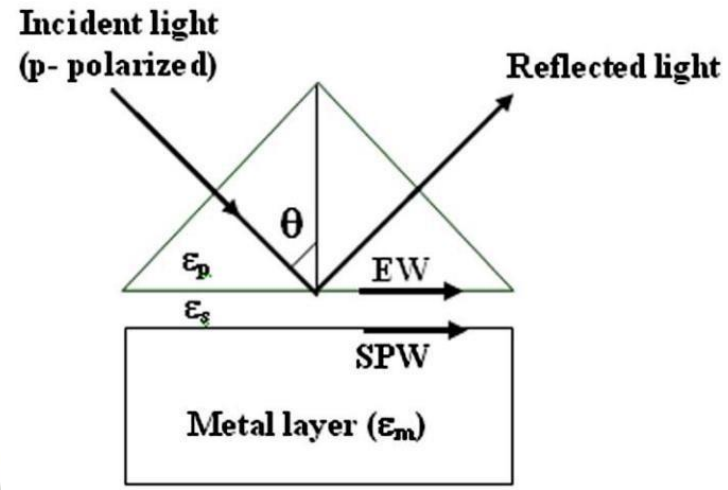

Figure 2-5 Otto coupling configuration for SPW excitation at the metal dielectric interface [32]

2.4.2 Kretschmann-Reather Configuratiion

This configuration is very similar to that of Otto configuration as it is an improvement of the Otto configuration. Kretchmann and Reather figured that if the prism is in direct contact with the metal and the metal layer was made thin enough(50nm), the evanescent field (generated through ATR at the prism metal interface) can radiated through the thin metal to excite surface plasmon waves that would propagate along the metal- dielectric interface(Figure 2-6).

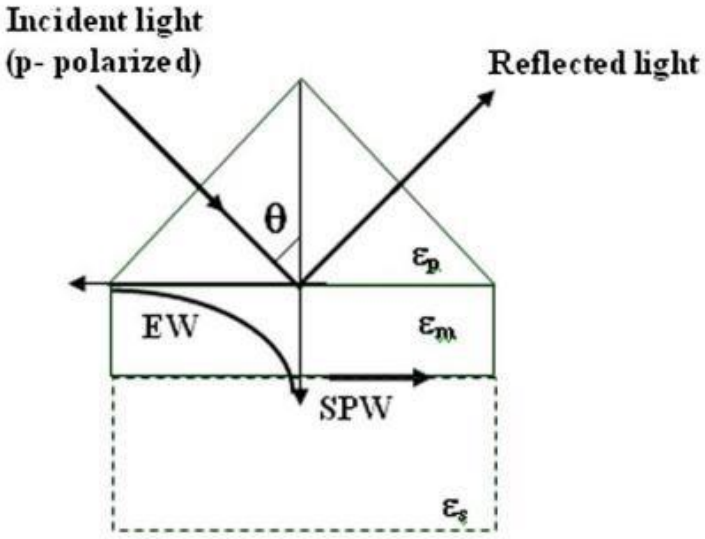

Figure 2-6 Krestchmann and Reather coupling configuration for SPW excitation at the metal dielectric interface [32].

However, excitation of SPW has a different approach. When p polarized light wave propagates through a high refractive index prism and impinges on th prism metal interface an an angle greater or equal to the critical angle $\theta_{ATR,}$ an evanescent wave is generated and propagates along the prism metal boundary.

The wave vector of the evanescent wave (K_{ev}) is eqaul to the lateral component of the wave vector of the incident light wave. Excitation of surface plasmon wave occurs only when, at a particular incidence angle, θ_{res}, the propagation constants of both evanescent and surface plasmon waves match. At this stage, SPW resonates with the evanescent wave which in mathematical terms is

$$\square \sqrt{\square}_p \sin\square \square_{res} - \square\square\square \square \square_{m\,s} \square^{\frac{1}{2}} \qquad 2.5$$

c c □□ □□ms □

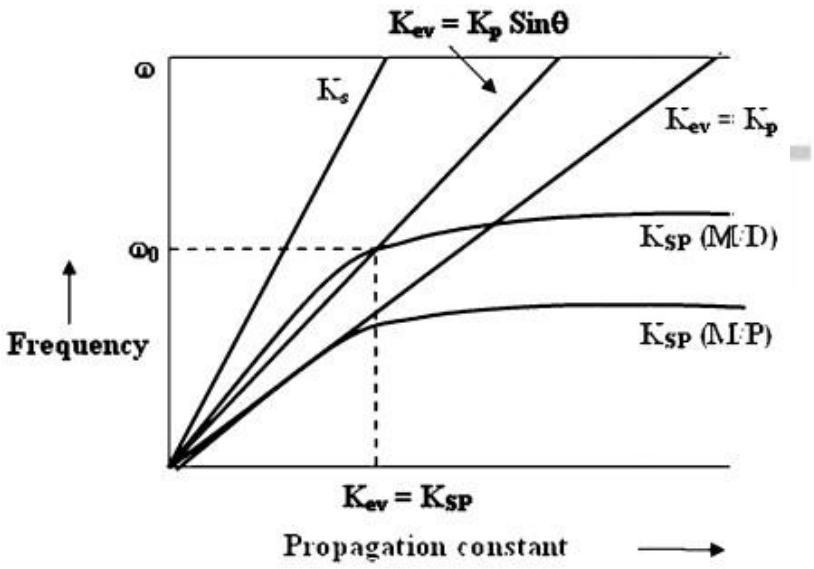

Figure 2-7 Dispersion curves for direct light wave in dielectric (K), evanescent Wave (K_{ev})for $\theta = \theta_{ATR}$ and θ =90, surface plasmon wave K_{SP} at metal dielectric interface (M/D) and at metal-prism interface (M/P) [32].

Therefore as illustrated in figure 2-7, when the propagation constant of the evanescent wave(K_{ev}) is equal to the lateral component of the p-polarised incident light wave propagation vector($K \sin_p \square_{res}$) at a particular resonant angle($\square_{res}$) and frequency($\square_o$) will have enough momentum to excite a surface plasmon wave with an equivalent propagation constantK_{sp}at the metal dielectric interface. There are no other excitations of SPWs at the metal prism interface because the conditions necessary for that to happen are parallel.

2.5 Grating Coupler

Alternatively, SPW can be excited using gratings on a metal surface as shown in Figure 2-8. The incident light inpinges on the gratings and is defracted into multiple paths. However, if any of the wave vectors of the difracted ligth is parallel to the surface grating and has matching propagation constants as the SPP [39], excitation of SPW occurs as described in the equaion below

$$\sqrt{\varepsilon_p}\sin\theta = m\frac{2\pi}{\Lambda} = K_{sp} \quad 2.6\,c$$

m represents the diffraction of order and Λ is the grating period. Interestingly, the incident light on the grating directly illuminates the surface of the metal thus requiring the sample dielectric to be optically transparent to enable light pass through it [40]. The reverse of using SPWs to generate light using the grating coupler is possible [41].

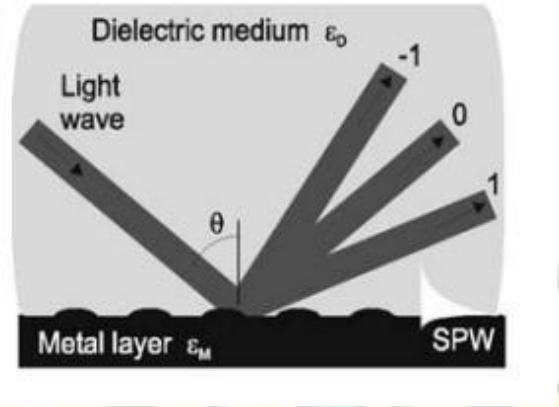

Figure 2-8 Grating couper configuration[31]

2.6 Fiber Optic Waveguide Coupler

Fiber optic wave guide couples possess similar basic characteristics to Kretschemann-Reather's prism coupler configuration where the prism is replaced with a fiber core. Figure 29 illustrates a typical fiber with its middle cladding portion etched off with a symetrically metal coated core.

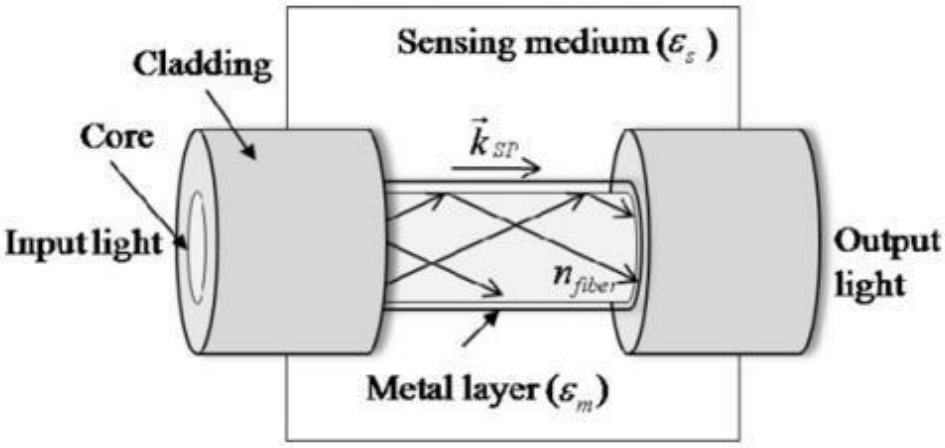

Figure 2-9 Wave guide coupler configuration for SPW excitation[39].

Lght guidance in the fiber core is very similar to that using the high refractive index prism; by total interna reflection(TIR).

When light, usually a polychromatic (white light), from a source is launched into one end of the fiber, TIR takes place for all multiple rays propagating with an angle ranging fron the critical angle to 90 degrees depending on the numerical aperture of the fiber and wavelength. An evanescent field is generated as a result which inturn excites the SPW to propagate along the core metal interface.

SPW excitation strongly depends on the wavelength and mode of light, fiber geometry and metal layer properties. Multimode coupling mechanism will be different from single mode coupling just like how straight and tappered will show different strengths of light coupling depending on the depth of penetration of the evanescent field [42-45]. At this stage, SPW resonates with the evanescent wave which in mathematical terms is

$$\frac{\omega}{c}\sqrt{\varepsilon_p}\sin\theta_{res} = \frac{\omega}{c}\left(\frac{\varepsilon_m \varepsilon_s}{\varepsilon_m + \varepsilon_s}\right)^{\frac{1}{2}} \qquad 2.7$$

Although prism coupler configurations are the most convenient in exciting SPWs, they are posses many optical and mechanical moving parts making them bulky and very chanllenging

to optimise and commercialise such configurations [46]. They are also not amenable to miniturasation which most a times is a requirment for remote sensing on a large scale.

However miniturization is achievable with fiber optic wave guides primarily due to their small diameters. Fiber wave guide coupling also have a couple of demerits such as the inability of one to control the angle of incidence which is possible with prism based coupling configuration. Consequently, this makes the resonance curve in the loss spectrum broader resulting in relatively lower sensitivity and detection limits.

2.7 Concept of Surface Plasmon Resonance Bio Sensing

Alluding to the fact that a larger portion ot the SPW field is concentrated in the dielectric, changes in the refractive index of the dielectric invariably changes the propagation constant of the SPW. This relationship between refractive index and SPW propagation constant is the underlying operational principle of affinity SPR bio sensors.

The biosensing process involves the capture of analytes contained in the liquid sample by biomolecular recognition elements(antigens) immobilized on the metal surface that target the analytes. The binding of atingens and analytes causes a localized increase in the refrative index of the sample close to the metal surface which consequently increases the propagation constant of the SPW propagating along the metal surface(Figure 2-10). This change in the propagation constant of the SPW can be accurately measured by optical means.

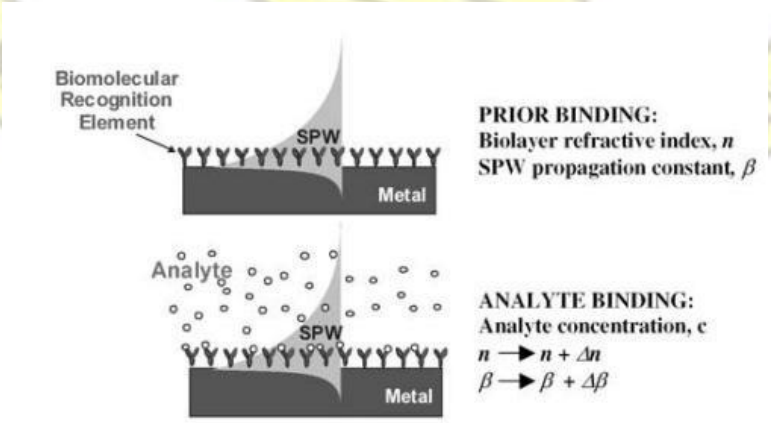

Figure 2-10Principle of SPR biosensing [31].

Changes in the magnitude of the propagation constant of the SPW depends on both the degeree of penetration of the magnetic profile of the SPW and the magnitude of change in the refractive index of the sample resulting from biomolecular binding events. The binding induced change in the propagation constant of the SPW is proportional to the refractive index change and the depth of the area within which the change occurs.

2.8 Interrogation of Surface Plasmon Waves

SPR manifests its self when SPW couples with the evanescent wave(generated for the incident light wave) inducing a resonant transfer of energy from the evanescent wave to the SPR. Consequently, the strong concentration of the SPW in the dielectric makes it very sensitive to changes in the optical properties of the dielectric [24].

This interaction between the SPR and the incident light wave alters the properties of the light such as polarization, phase, amplitude and spectral distribution. Variations in these characteristics can be correlated with changed in the propagation constant of the SPW [24]. Therefor binding induced changes in the refractive indexat the surface of the transduces(metal) and consequently the propagation constant of the SPW can be determined by measuring changes in those light wave characteristics [31]. The folowing detection modes are commonly used;

- Intensity interogation of the reflected optical wave at resonance [8, 9, 47]
- Angular interrogation of the optical wave at resonance [48, 49]
- Wavelength interogation of the optical wave at resonance [50-52]
- Phase interogation of the optical wave at resonance [53, 54]
- Polarization interogation of the optical wave at resonance [55]

2.8.1 Intensity/Amplitude Interrogation

This interogation method involves measuring the change in intensity of the light wave after its interaction with the SPW at a fixed wavelength and angle of incidence. The coupling of the evanescent wave to the SPW transfers energy resonantly to the SPW consequently registering a change in ligth wave intensity.

The largest change in ligth intensity indicates the wave length and angle at which the strongest coupling occurred. Much progress has been made in this area primarily focusing on improving performance and increasing throughput [56-68]

2.8.2 Angular Interrogation

This form of interogation provides a way to determine the component of the light wave vector parallel to the metal surface which excites the SPW. The coupling strength of the SPW to the evanescent wave is mesured at a constant wavelength while varying the angle on incident lightwave until the an angle yielding the stronges coupling. The strongest coupling is indicated by a peak in the plots of reflectivity or attenuation(loss) spectro.

2.8.3 Wave Length/Spectral Interrogation

This interogation approach employs a fixed angle of incident light while variying it's wavelength to finally determine the wavelength yielding the strongest coupling of the component of the light wave vector parallel to the metal surface propagting at the same rate as the SPW. The wave length at which the strongest coupling occurs would register the highest loss or the lowest reflectivity as the resonant transfer of light energy from the evanescent wave to the SPW. Some published work include [49, 69-76]

2.8.4 Phase Interrogation

This interogation method involves measuring the shift in phase of the light wave after its interaction with the SPW at a fixed wavelength and angle of incidence. The coupling of the

evanescent wave to the SPW transfers energy resonantly to the SPW consequently registering a change in ligth wave phase. The largest phase shift indicates the wave length and angle at which the strongest coupling occurred. Much research based on phase interogation have been puplished [54, 77-80].

2.8.5 Polarization Interrogation

This interogation method involves measuring the change in the polarisation of the light wave after its interaction with the SPW at a fixed wavelength and angle of incidence [31]. The coupling of the evanescent wave to the SPW transfers energy resonantly to the SPW consequently registering a change in ligth wave polarisation. The largest change in ligth polarisation indicates the wave length and angle at which the strongest coupling occurred.

2.9 Performance Characteristics

The major characteristics in realation to performance that enable the description of SPR bio sensor in measurable quantities include sensitivity, accurace,precision and the lowest detection limit.

2.9.1 Sensitivity

Sensitivity of an SPR bio sensor is the ratio of the change in sensor output,P,(such as the angle of incidence, wavelength, intensity, phase and polarization of the light wave intera) to the change in the quantity to be measured (analyte concentration). Furthermore, sensor sensitivity is dependent on two factors; sensitivity to refractive index changes produced by the analyte binding to biomolecular receptor elements on the surface of the sensor, S_{RI} and efficiency ,E, with which conversion of analyte concentration c, to change in refractive index, n. mathematically;

$$S \frac{\partial}{\partial} \frac{\partial}{\partial} P n S E_{RI} \quad 2.8$$
$$\partial \partial nc$$

The properties of both target analyte and recognition elements as well as their interaction contribute to the efficiency E of the sensor. Refractive index sensor sensitivity can further be broken into two components;

$$S_{RI} \frac{\partial}{\partial} \frac{\partial}{\partial} P \partial Re \partial \partial \partial \partial SS_1 \quad 2 \quad 2.9$$
$$\partial Re \partial \partial \partial \partial n$$

S_1 represents the contribution of the choice of coupling and interrogation method of the SPW[81, 82], S_2 which is independentt of the contributions from coupling and interogation methods describes the contributions to sensitivity by refractive index changes.

Further more, indepth studies in to sensitivities of SPR devices are available [83-85]. Sensitivity to refractive index changes obtained for SPR devices using angular interogation was found to increase as wave length decreases [85], conversely that which was obtained for SPR devices using wavelength and intensity interogation was found to increase with increasing wave length [86]. Additionally, silver metal layers slightly gave better performance than gold metal layers when interogation techniques such as wavelength and intensity was used [84, 86].

2.9.2 Resolution

Sensor resolution is an important attribute of SPR sensors that measures the smallest change in the bulk refractive index that produces a detectable change in the sensor output. The degree of detectable change in sensor output depends on the output noise level (level of uncertainty) of the SPR sensor output.

Intensity interrogation technique, when applied to study the relationship between the light wave and the SPW, its resolution will be limited by the noise in the intensity of the detected light. Same applies to the other interrogation techniques. Major noise sources include fluctuations in the light intersity emitted by the light source, shot noise from photon statics and noise in conversion of light intensity fo electrical signals by the detector. Consequently, systematic studies have been made to determine the influence of temperature and the afore mentioned noise sources on resolution [31, 87, 88].

2.9.3 Accuracy and Precision

Accuracy as the name implies, describes the dgree to which the sensor output represents the true value of change in the measurand (analyte concentraion) [31]. Precision on the other hand, describes the way in which repeated measurements conform to themselves without a reference to any true value [31].

2.9.4 Limit of Detection and Minimum Resolvable Surface Coverage

The lowest limit of detection indicates the least concentration of analyte required to yield a sensor output equivalent to three standard diviations of standard sensor output results for a blank sample [82]. The level of acuracy for the limit of detections can be increased if parameters pertaining to interactions between biorecognition elements and target analytes are known [30].

2.10 Evolution of Fiber-Optic SPR Sensors

There are many SPR sensor configurations (Figure 2-11) that have been developed over the past two decades. Some of these are; symmetrical structures, such as a simple metal coated optical fibers with or without remaining cladding over a particular section [89-91], tapered fiber [92, 93], structures without any symmetry, such as side-polishedfibers (or D-shape fiber)

and one-side metal coated fibers with and without remaining cladding [94-96], and structures with modified fiber tips with flat or angled structures [97, 98].

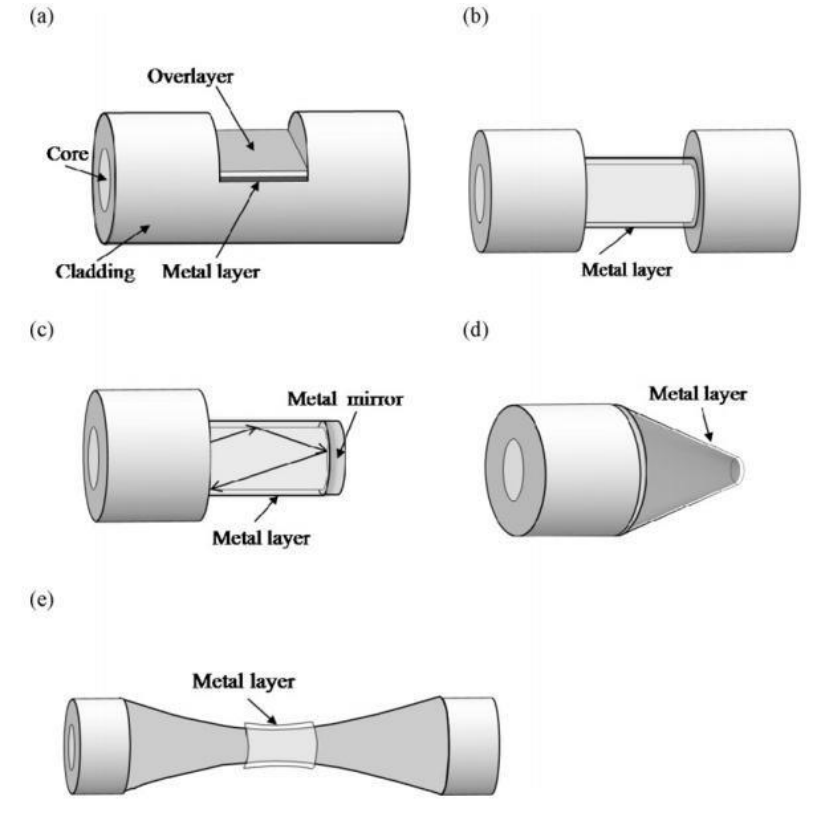

Figure 2-11General SPR fiber-optic sensor schematics with (a) D-shape fiber, (b) cladding-off fiber, (c) end-reflection mirror, (d) angled fiber tip, and (e) taperedfiber [39].

In the early nineties, the use of fiber optic technology for sensing become a main focus for research and development. One of the first reported fiber optic SPR sensors was by [99] describing sensitivity and dynamic range results for the measurement of sucrose concentration in aqueous environments. They followed up with a more sensitive four layered fiber sensor with inproved dynamic range in comparision to their precious three layered sensor [100]. A short while after, a paper reported the use of monochromatic light for SPR excitation at the tip of a single mode fiber using polarization interrogation [101].

A fiber optic chemical sensor was reported about the same time by Jorgenson and Yee which used a probe and a multimode fiber with white light as a source. Numerical and experimental results show the capability of the sensor to measure bulk refractive index changes, film

refractive index and thickness [51]. Multi mode fibers are generally sensitive to mechanical disturbance thereby altering light intensities over time. In that same year, a large ranged 'inline' fiber sensor was presented [36]. Mar, Jorgenson and others demonstrated for the first time in 1993 the monitoring of calcium arachidate Landmuir-Blodgett film deposition in multiple layers discovering a way to calculate film thickness using changes in spectra [102]. As research focus narrowed down to improving sensitivities and operational range, reports such as [103] demonstrated sensitivites in the order of 10^{-5} and operational range of between 1.25RIU(refractive index unit) and 1.40 RIU using a thin high refractive index over layer. Additionally, the range is extendable to 1.70 in the fiber core is saphire. Soon after, remote capabilites where incorporated into the sensor first by [104][19]. The use of monochromatic light sources and single mode fiber increased the sensitivities(in the order of 10^{-4}) of fiber sensors as reported by [91] and later by Homola in [105] using a polished single mode optical fiber and a thin metal overlayer. However they are more challenging to fabricate even though they are more sensitive, accurate and contain less noise.

Research into the self assembled monolayers(SAMs) such as n-alkanethiol, as part of the evolution of fiber optic sensors, paved way for silver to be exploited more in its use in fiber sensor fabrications [105]. As silver is chemically unstable this brough about giant leaps forword in silver film protection. None the less, silver gives a narrow transmission spectrum thus enabling high resolution to be achieved. Gold on the other hand is chemically stable and can be used to attain high sensor sensitivity figures [39]. Aditionally, a sensor based on SAM was found to be very stable and did not loose its performance characterics as it aged. This sensor was aplied in gas detection with a polyfluoroalkylsiloxane as the dielectrice deposited over the SAM [106].

Another major leap came with the introduction of metal coated tappered fiber for refractive index sensing[107]. Research suggested that tappered fiber based sensors were easier to

fabricated with better sensing efficiency as compared to polished type fiber sensors [107]. A fiber optic sensor with its dynamic range reduce using a zirconium acetate on a silver metal surface was reported by Lin *et al* [108]. The deposition of the analyte on the metal surfacewas by way of sol-gel method.

Soon after, an alternative approach to theoretically analyse suface plasmon excitation in optic fiber based sensors was developed [109]. This approach involved the numerically evaluating the transmission parameters such as sensitivity using loss optical power loss resulting from the coupling between the evanescent field and the SPW. Energy conservation consederations reconciled experimental wth theoretical results making them practically applicable.

Further strides where made when long periodic gratings(LPGs) where introduced to couple light from the central core to the cladding while tunning the light wave phase to match that of the SPW. He et al demonstrated numerically that it was possible to use LPGs to excite SPWs resonantly coupling a particula cladding mode to the SPW [110].

Tang also reported the use of a SPR sensor employing LPG and self assembled gold colloids in sensing concentrations of chemical solutions in addition to detecting biomolecular binding events at a nano scale level. Registered sensitivity values of -23.45nm/RIU were made making them more sensitive than conventional long grating fibers in addition to its simple structure and user friendliness [111].

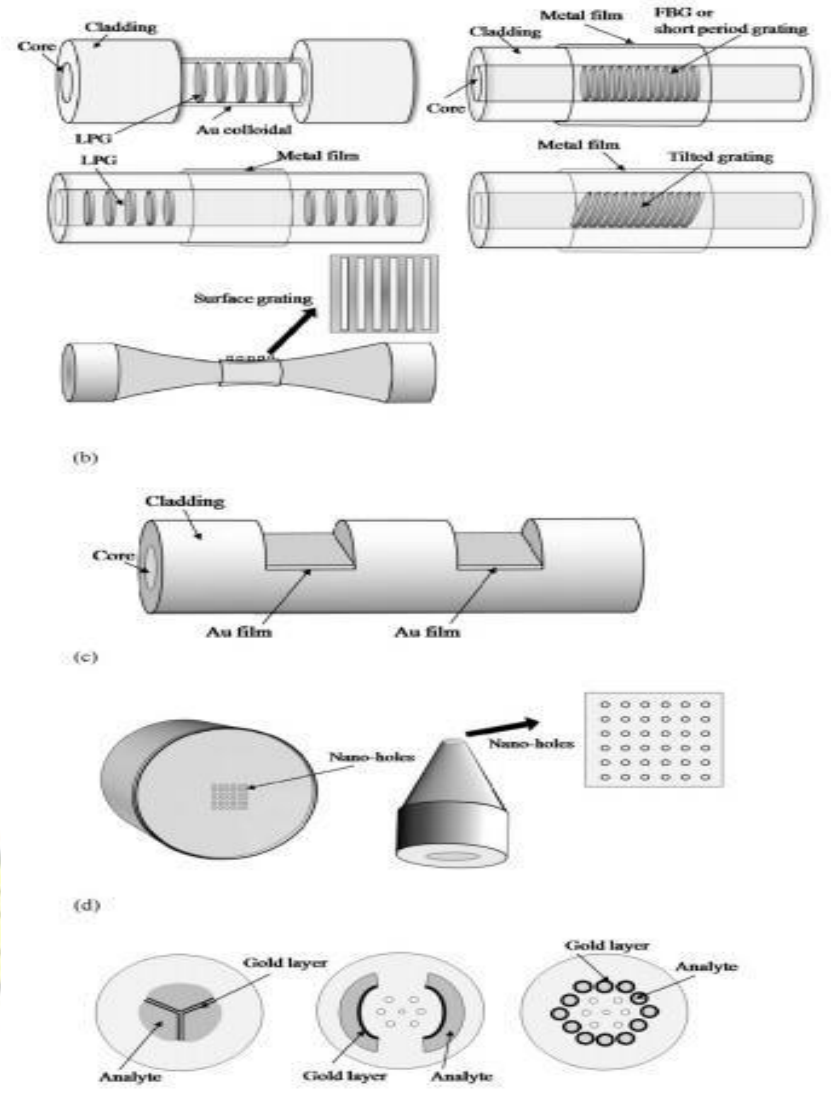

Figure 2-12 Examples of SPR fiber sensors (a) with a long period grating (LPG), a short period grating (or fiber Bragg grating (FBG)), LPG pair, tilted grating, and metal surface grating, (b) with a cascaded sensing region, (c) with nano-holes on a fiber tip that is flat or angled, and (d) with photonic crystal fibers [39].

Fiber bragg grating configurations require very special fiber designs for SPW excitation. Nemova and Kashyap reported that FBGs do not readily couple to the core mode to the cladding mode hence the need for a special design [112]. Nonetheless, an SPR sensor based on FBG configuration with hollow core have been reported [113] alongside tilted fibergratings [114] and metalic brag gratings [115]. Even though these configurations show sharp resonance dips and good SNR values, they have slightly decreased sensitivities(10^2 - 10^3 nm/RIU) as compared to conventional SPR sensors.

Optical structure	Characteristics	Detection IR range	Wavelength	Sensitivity
Metallic grating	SMF, tapered, Au, metal surface grating,	1 ~ 1.41	1200 ~ 1500 nm	500 nm/RIU
Two region coating	SMF, Au, temp. correction, selfreferencing	1.32 ~ 1.36,	600 ~ 1400 nm	$1 \times 10^{-4} \sim 5 \times 10^{-5}$ RIU
	MMF, Au, cascade sensing layer	1.3333 and 1.3338	500 ~ 1700 nm	2×10^{-5} RIU
Absorption layer	Tapered fiber, silver and praseodymium oxide		450 ~ 600 nm	
Dual light source	MMF, two LEDs	1.333 ~ 1.3616	609.6 and 675.9 nm	5.2×10^{-4} RIU
Modified fiber end	MMF, GIF, hole milling	1.33 ~ 1.376	440 ~ 760 nm	533 nm/RIU
Photonic crystal fiber	Three hole, Au, dielectric layer	1.33 and 1.34	500 ~ 600 nm	10^{-4} RIU 7×10^{-6} RIU
	Hollow core Bragg fiber, honey comb PCF, Au			
	Micro-structured optical fiber, Au			10− RIU/% (intensity)

Table 2.2 Performance of novel SPR based fiber-optic sensors [39].

In recent times, reserchers have proposed many designs of SPR sensor based on photonic crystal fiber(PCF) configuration. These configurations support single mode wave propagation and facilitae excitaion of SPWs by Gaussian - like leaky modes [116][72]. These configurations enable efficient phase matching while maintaining thier high sensitivity making an ideal choice for portable SPR biochemical sensors. Furthermore, an enhanced version with integrated micro fluidics is available [117].

This enhanced configuration comprise large metal coated channels housing the analytes arranged around and close to the core through whichb a core guided single mode wave propagates. Kautokorpi et al reported a theoretical analysis of a three hole micro structured optical fiber with gold deposited as a layer in them. Results indicated small optical loss and a resolution of 10^{-4} could be obtained [118]. Many other SPRsensor types based on this configuration have been reported [119, 120]

2.11 Micro and Nano-Structured Optical Fiber Sensors

Micro- or nano-structured optical fibers cover a wide range of optical fibers, including PCFs and some fibers with nano-structures at the end or side of optical fibers. With regard to PCFs, according to the cross-sectional distribution of the dielectric function, PCFs can be categorized as follows: photonic-bandgap fibers (PCF that utilizes the photonic bandgap and the defect mode), holey fibers (PCF with air holes along the axis of light propagation), holeassisted fibers (PCF consisting of a conventional higher-index core with air holes), and Bragg fibers (photonic-bandgap fiber with concentric rings of different refractive indexes).

Fabrication is a key factor in the designing and developing of new fibers. The PCF technology not only provides a greater manupulation of the fiber design, but also allows fibers to be made from just a single material, eliminating needs for two thermally, chemically and optically compatible glasses to form their core and cladding, as otherwise required within conventional fibers. A wide range of materials has been used to fabricate PCFs, including chalcogenide , lead silicate , bismuth silicate and tellurite glasses , and even polymers [121] . The use of different materials opens up agreater degree of freedom for the fiber design. The stack-and-draw procedure was devised by the group from the University of Bath and is the most used in PCF fabrication. This technique provides high versatility, allowing complex lattices to be assembled from individual stackable units of the correct size and shape. Solid, empty or doped glass regions can be easily incorporated. It involves no chemical process .It is worth noting that the possibility of using new materials, with lower melting points, facilitates the use of other techniques apart from capillary stacking for preform production. In fact, other techniques such as extrusion [122], built-in-casting [123] and drilling [124] have also been reported.

2.12 Conclusion

This thesis focuses on the use of micro structred fibers for bio sensors for aquoeus enviroments. Attemps to solve challenges such as non specific interactions between non target analytes and

the sensor surface and also background refractive index variations due to temperature and humidity was made using a self refrencing technique [125][203]. This technique involves the use of fiber structures that support two surface plasmon; long range surface plasmons (LRSP) and short range surface plasmons(SRSP) [126, 127].

With the help of an additional layer between the sample and the metal layer a symmetric refractive index profile is created [128] that supports both LRSP and SRSP. The different penetration depths of the two SP types consequently enables diffrenciating surface interactions of intrest from non target interaction and also preventing interference from background refractive index variations [129].

3 CHAPTER 3 : METHODOLOGY

3.1 Introduction

In this chapter, the design of the proposed SPR bio sensor is presented in detail. The theoretical description of the model in terms of its numerical characterisation to match real life operations as well as its performance metrics is elucidated. All numerical tools employed in the realisation of the bio sensor are included in this chapter.

3.2 Finite Element Method

In this thesis, finite element method(FEM) [130, 131] is used as a numerical tool to investigate the propagation characteristics of modes. FEM allows the solution of a large class of partial differential equations without any limitation by geometry. Futhermore, the use of FEM necessitates the division of the PCF cross section into homegenous subspaces(mesh) within each Maxwell's equations are solved, accounting for adjacent subspaces. For fibres, as in this case, the use of triangular subspaces provides a good approximation for its circulat nature [132]

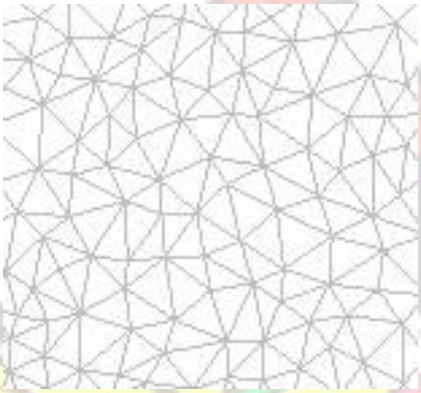

3.1 FEM mesh

Considering the unique structures of PCFs a full vector FEM formulation would be required study wave propagation through fibers with arbitrary air filling fraction. Full vectorial FEM incorporates anisotropic perfectly matches layers(PML) enabling one to solve for as many modes as desired in a single run without iterating[133]. Analysis of leaky modes is also possible with PMLs. As such, both dispersion and loss properties can be determined in a single run. In the case of propagation mode computation, FEM creates a matrix that numerically approximates the partial differential operator of the problem transforming it into numerical eigen-value problem, which is then solved using numerical algebra techniques.

3.2.1 Implementation of FEM on PCFs

The study of hybrid mode and polarisation dependant wave propagation requires a full vectorial analysis. Consider an optical wave guide with an arbitrary cross section in the x-y plane, has a full vectorial wave equation derived from Maxwell's equations in the form of

$$\nabla \times [p] \nabla \times H - k q_0^2 [q] H = 0 \qquad 3.2$$

With H representing the electric field **E,** or magnetic field **H**, with permeability tensors $[p]$ and $[q]$ alternatively written as

$$[p] = \begin{bmatrix} p_x & 0 & 0 \\ 0 & p_y & 0 \\ 0 & 0 & p_z \end{bmatrix} \qquad 3.3$$

$$[q] = \begin{bmatrix} q_x & 0 & 0 \\ 0 & q_y & 0 \\ 0 & 0 & q_z \end{bmatrix} \qquad 3.4$$

Where $p_x = p_x = p_x = 1$, $q_x = n_{x y}^2 = n_{y z}^2 = n_z^2$ for the electric field component ($\nabla \times \mathbf{E}$) and

$\frac{1}{q_x} = \frac{1}{q_x} = \frac{1}{q_x} = 1, \frac{1}{p_x} = n_x^2, \frac{1}{p_y} = n_y^2, \frac{1}{p_z} = n_z^2$ for the magnetic field component ($\nabla \times \mathbf{H}$).

Finally, the expressions n_x, n_y and n_z are refractive indices in the x, y and z directions respectively.

3.3 Perfectly Matched Layer

These are additional spaces/domains that do not reflect incident radiation but rather absorbs them. As part of the model, its specified to be made of a different absorbing material of varied

thickness. This absorbing material must have matching anisotropic permeability and permitivity with the physical medium outside the PML such that ther are no reflections.

Maxwell's equations can be usd to formulate the PML by introducing a complex valued coordinate transform under the additional requirement that the wave impedance should remain unaffected.

3.3.1 Mathematical Analysis of FEM with Anisotropic-Type PML

By using the Maxwell's curl equations [134] we can derive the vector wave equations for magnetic field, ***H***, and electric field, ***E***, as shown;

$$\nabla \times \mathbf{E} - \frac{i\omega}{c}\mathbf{H} = 0 \qquad 3.5$$

$$\nabla \times \mathbf{H} - \frac{i\omega}{c}\varepsilon_r \mathbf{E} = 0 \qquad 3.6$$

By dividing the equation 3.6 by ε_r (relative permittivity of the medium) and then take the curl. Then first equation used to eliminate ***E*** and the result is:

$$\nabla \times \left(\frac{1}{\varepsilon_r}\nabla \times \mathbf{H}\right) - \frac{\omega^2}{c^2}\mathbf{H} = 0 \qquad 3.7$$

To use an anisotropic-type PML, [132, 135] equation 3.7 takes this form

$$\nabla \times \left(\frac{1}{s_1}\nabla \times \mathbf{H}\right) - k_0^2 s_2 \mathbf{H} = 0 \qquad 3.8$$

$$\nabla \cdot (n^2 \mathbf{E}) = 0$$

With $c.k_0$, and

$$[s] = \begin{bmatrix} \frac{s_z s_y}{s_x} & & \\ & \frac{s_x s_z}{s_y} & \\ & & \frac{s_x s_y}{s_z} \end{bmatrix} \qquad 3.9$$

Where k_0, is the free-space wave number and n is the refractive index of medium .The *del* operator, ∇ is defined as [136]

$$\nabla = \hat{x}\frac{\partial}{\partial x} + \hat{y}\frac{\partial}{\partial y} + \hat{z}\frac{\partial}{\partial z} \qquad 3.10$$

The parameters S_x, S_y and S_z are the complex-valued coordinates scaling parameters. By assigning suitable values to these, you can obtain a PML that absorbs waves traveling in a particular direction.

PML parameter	PML region		
	1	2	3
S_x	α	α	1
S_y	α	1	α
S_z	1	1	1

Table 3.1 PML parameters

The PML parameters S_x, S_y and S_z are given in table 3.1, and since the wave propagation is assumed to be along the z direction S_z will be set unity. The values below represent a PML that absorbs a wave traveling in the x direction. $s_x \square\square$,$s_y \square 1, s_z \square 1$

Where $\square\square 1\square j\square_j$ for leaky-mode analysis.

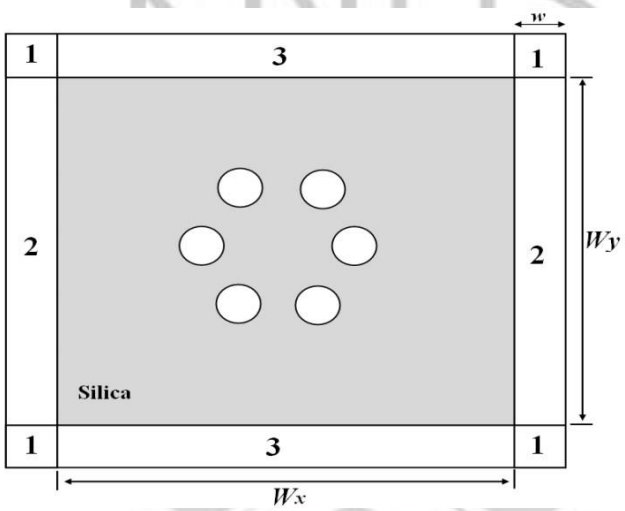

Figure 3-1Schematic of a PCF surrounded by PML

Magnetic field attenuation [313] in the PML regions can be regulated by achieving an appropriate value for $\square_j$ using

$$\square \square\square_{jjmax} \square \square\square \square\square \qquad 3.11$$
$$\square \square\square$$

$\square$ represent the distance from the beginning of the PML while $\square$is the thickness of the PML. The subscript "max" denotes the maximum value.

3.4 Numerical Modelling and Sensor Design

3.4.1 Effective Refractive Index

In homogeneous transparent media, the refractive index *n* can be used to quantify the phase change per unit length: that phase change is *n* times higher than it would be in vacuum. The effective refractive index n_{eff} has the same meaning for light propagation in a waveguide and

depends not only on the wavelength but also on the mode in which the light propagates. The effective index may be a complex quantity in which case the imaginary part describes gain or loss [137].

3.4.2 Confinement Loss

When wave guidance is not completely confined to the central core by the finite number of layers of holes in PCFs, leakage from the core to the outer matrix material occurs resulting in loss of electromagnetic energy to the cladding. These losses are called confinement losses. Furthermore, coupled mode theory is underlying principle employed for sensing. At the resonance point, the core guided mode couples with the surface plasmon wave because their propagation constants match resulting in much loss of energy from the core mode to the plasmon mode. A change in either the resonant wavelength or the intensity of the two modes is the measurable tool. The imaginary part of the complex refractive index (n_{eff}) is used in determining confinement losses (L) [119] using

$$\text{Confinement loss} = \frac{40}{3.12 \ln(10)} \text{Im}(n_{eff}) \approx 8.686 k_0 \text{Im}(n_{eff}) \quad \text{dB/m}$$

Where Im n_{eff} is the imaginary part effective refractive index and λ (nm) is the operating wavelength ($k_0 = 2\pi/\lambda$).

3.4.3 Material Dispersion

All materials are dispersive in nature; *i.e.* the refractive index is wavelength dependent. Spectrally, a pulse of light is associated with a superposition of a range of frequencies, centered on the frequency of the modulated light source. Due to material dispersion, each spectral

component of the pulse will propagate at different speeds, resulting in pulse spreading and deformation [138].

The background material, pure silica, is modelled using the Sellmier equation [139]:

$$n(\lambda) = \sqrt{1 + \frac{B_1\lambda^2}{\lambda^2 - C_1} + \frac{B_2\lambda^2}{\lambda^2 - C_2} + \frac{B_3\lambda^2}{\lambda^2 - C_3}} \quad 3.13$$

Where n and λ is the index of refraction wavelength respectively, $B_{(i = 1,2,3)}$ and $C_{(i = 1,2,3)}$ are Sellmeier coefficients. The values of the coefficients are defined as follows B_1=0.696166300, B_2=0.407942600, B_3=0.897479400, C_1=4.67914826×10^{-3}μm^2, C_2=1.35120631×10^{-2} μm^2 and C_3= 97.9340025 μm^2 and thus the material dispersion of the fibre has been accounted for. Gold permittivity is modelled from Johnson and Christy data [140].

3.4.4 Birefringence

The breaking of symetry of optical fibers introduces two orthogonally polarized modes propagating at different phase velocities. This is termed birefringence. Perfectly circular core fibers are no exceptions because unavoidable geomety deviations and stresses suchas bending and twistind breaks the perfect symery.

The flexibility offered in the manufacturing of PCFs provides an opportunity to delibrately introduce enough birefringence required to achieve a specific goal. For instance, in this thesis, birefringence was used to introduce the concept of multiple analyte sensing of a proposed bio sensor. Its structural symetry was broken by introducing air holes of different radii near the core area and in another case by elliptical air holes.

The breaking of symetry results in one axis with a larger mode index(slow axis) while the other has a lower mode index(fast axis). Hence the slow axis has smaller dispersion as compared to the fast axis. Mathematicall, birefringence can be express as

$$B = |n_x - n_y| \quad 3.14$$

With n_x and n_y being the effective indices of each fundamental mode (HE_{11}^x and HE_{11}^y).

3.5 Numerical Tools

There are three numerical tools used in this thesis. They are as follow:

MATLAB® versionR2012a is a high-level language and interactive environment for numerical computation, visualization, and programming. Its numerical computation capability has been employed in the evaluation of performance parameters such as interrogation modes, birefringence, and confinement loss in this thesis. The tools, and built-in math functions allow multiple approaches in order to arrive at a solution faster as opposed to spreadsheets or traditional programming languages [141].

OriginPro is a proprietary computer program for scientific interactive graphing and data analysis. It support 2D/3D plot types graphing statistics, signal processing, curve fitting and peak analysis are all forms of data analysis in origin. Files are imported in origin in various formats such as ASCII text, and .mat files.

Comsol Multiphysics is a powerful software package that can perform eigen-frequency and modal analysis. Comsol Multiphysics employs the proven finite element method (FEM). The software runs the finite element analysis together with adaptive meshing and error control using a variety of numerical solvers. With this software you can design Photonic crystal fibers easily by defining the sub-domains and boundary conditions with correct parameters and also

you can solve the problems for both electric field and magnetic field. Software also gives you visual option that as it shown in Figure 3-2 you can see the solutions at different angles with different transversal components (*x*, *y*, *z* component).

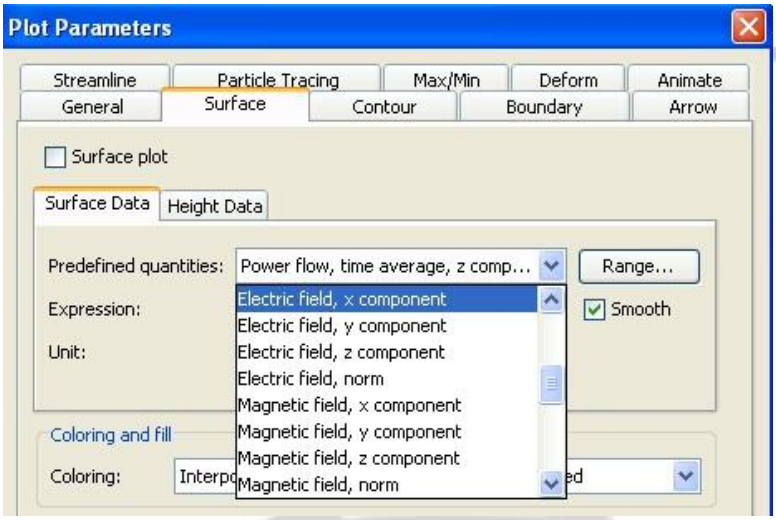

Figure 3-2 Option window of plot parameters

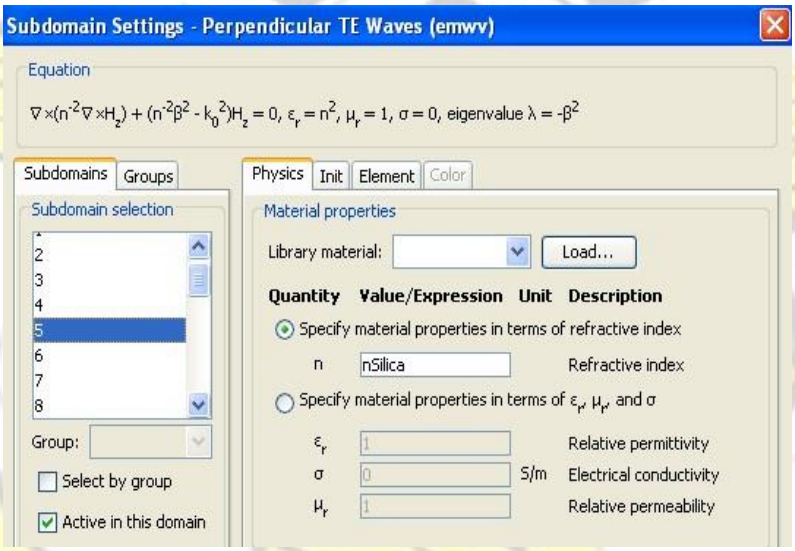

Figure 3-3Sub-domain settings window.

3.6 Modelling In Comsosl Multiphysics Version 3.4

To define PML in FEMLAB, introduce a new sub-domain representing an absorbing layer with anisotropic material parameters. The table below shows the relative permittivity, ε_r and the permeability, μ_r that is used for all the simulations.

ε_r (anisotropic)	[Lxx*2.1025 0 0 Lyy*2.1025 Lzz*2.1025]
μ_r (anisotropic)	[Lxx 0 0 Lyy Lzz]

Table 3.2 Pemeability and permitivity characterization

$$\text{Where, } L_{xx} = \frac{s \cdot s_{yy}}{3.15\, s_x\, s_y}, \quad L_{yy} = \frac{s \cdot s_{xy}}{s_z}, \quad L_{zz} = \frac{s \cdot s_{yx}}{}$$

Optical anisotropy is the property of being directionally dependent. Something which is anisotropic, may appear different, or have different characteristics in different directions. From the reasons explained above, when Hybrid mode analyses are made the software solves the problem for both *x* any *y* direction (HE_{11}^{x}, HE_{11}^{y}).

CHAPTER 4: RESULTS AND DISCUSSION

4.1 Introduction

This thesis proposes two biosensor designs in line with its objectives. The first is a highly birefringent compact photonic crystal fibre surface plasmon resonance biosensor**,** which is designed to be highly sensitive, easy to fabricate, amenable to integration and introduce the concept of multi analyte sensing using birefringence. The second design is an improvement of the first as it exhibits multiple analyte sensing capability with better sensitivity than the first.

Investigation of key performance parameters such as birefringence, confinement loss and sensitivity was done using full-vectorial Finite Element Method (FEM) with perfectly matched layers (PML) to vary structural parameters such as pitch, air hole diameter, gold thickness and refractive index of the analyte. The solver settings of FEM based on anisotropic perfectly matched layers (PML) enables any desired number of confined and leaky modes to be analysed. This analysis focuses on the fundamental modes HE_{11}^{x} and HE_{11}^{y}. Modal analysis of the fundamental mode has been performed on the cross section in the x-y plane of the PCF as the wave is propagating in the z – direction.

4.2 Highly Birefringent Bio sensor Design and Characterisation

Figure 4-1 shows the structure of the proposed novel highly birefringent PCF SPR bio sensor to be optimized for operation in aqueous environments. This bio sensor design consist of circular air holes of varying radii arranged in a hexagonal lattice structure with a small hole in the center. The large circular air holes, denoted by d_m are used to introduce birefringence into the structure. Tuning of the phase matching point of the core mode to the plasmon mode is achieved with the small circular hole at the center of the structure denoted byd_1. The presence of d_1 at the center of the structure also

lowers the refractive index of the core guided mode. The pitch denoted by Λ is the inter air hole spacing.

The two holes in the first ring distorts the perfect symmetry of the guided core mode thereby introducing birefringence into the module. The four large holes in the second are used to vary the amount of birefringence being introduced. Additionally, the second ring forms a cladding with low refractive index which enables wave guidance. The third ring comprise of two gold coated, of thickness t_{Au} large slots of same thicknessd_3 which house the analyte.

The slot gap, ds is set to be equal to d_1 throughout its study. Due to the birefringent nature of the proposed PCF SPR sensor, the slot design is important to give adequate cover for both HE_{11}^{x} and HE_{11}^{y} modes with gold layers to ensure efficient coupling with the plasmon mode.

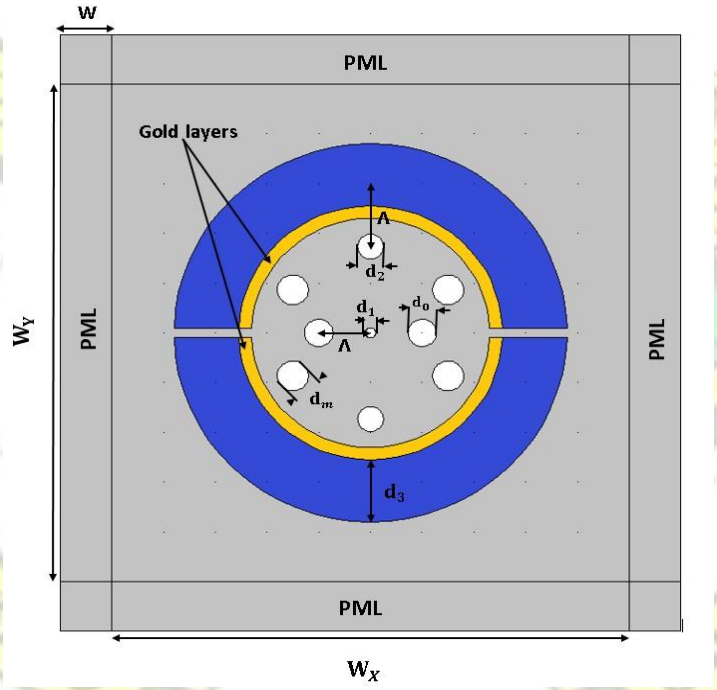

Figure 4-1Cross section of the proposed PCF SPR bio sensor showing various sections

The following structural parameters are used; Λ=1µm, d /1 □□ 0.30,d /0 □□ 0.55, d /2 □□ 0.50, d_m / □□ 0.6 and t_{Au} □ 40nm. The two large channels in the third ring are filled with

an aqueous analyte having a refractive index of n_{ana} 1.33(water) and the confinement losses for both fundamental modes, HE_{11}^{x} and HE_{11}^{y} are calculated. The whole process is repeated for another analyte with refractive index of n_{ana} 1.34 and the results for both processes are plotted.

4.3 Analysis of Structural and Performance Metrics

Our analysis begins with the investigation of the proposed PCF for good sensing capabilities.

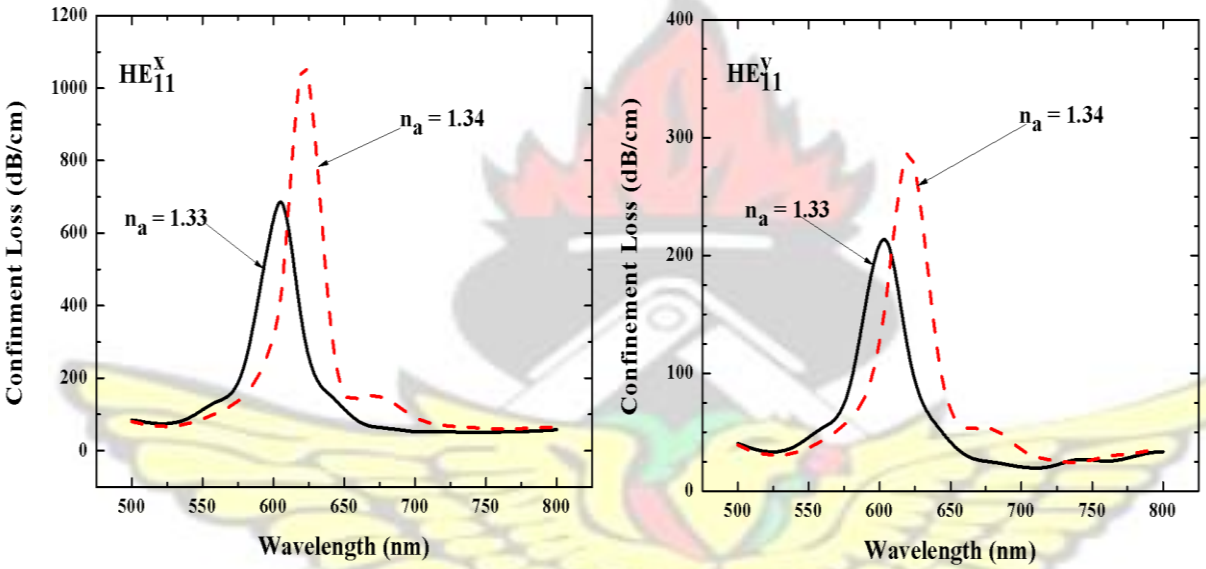

Figure 4-2 Calculated loss spectra of the fundamental modes HE_{11}^{x} and HE_{11}^{y} Loss spectra (solid curves) feature attenuation peaks corresponding to the excitation of plasmonic modes on the surface of metallized channels filled with aqueous analyte n_a = 1.33.

Figure 4-2 shows loss spectra for both fundamental modes, HE_{11}^{x} and HE_{11}^{y} with peaks corresponding to the excitation of plasmon modes on the surface of metalized channels filled with aqueous analyte n_{ana} 1.33 (solid line) and n_{ana} 1.34 (dash line). Figure 3 shows the magnetic field distribution for both HE_{11}^{x} and HE_{11}^{y} (fundamental modes), near the region of the first plasmon peaks of the proposed PCF SPR sensor.

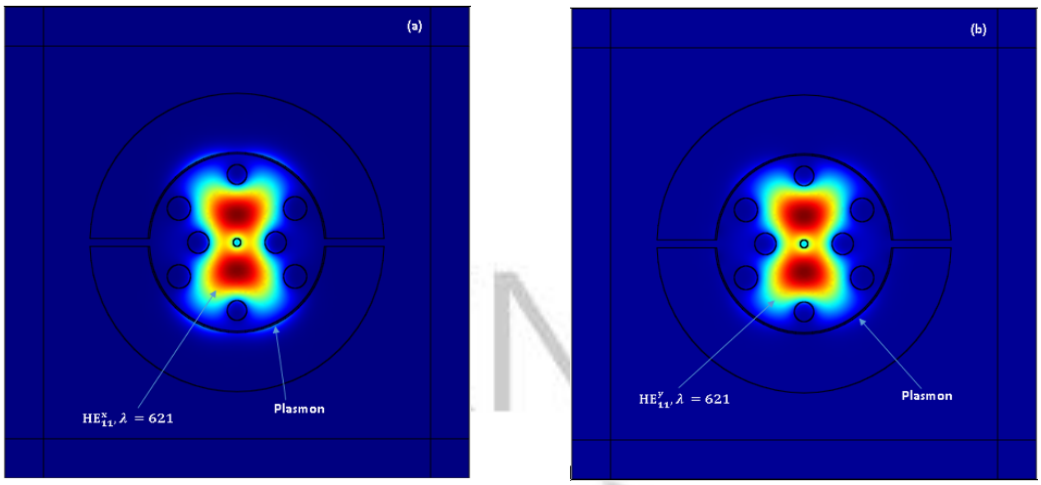

Figure 4-3 Magnetic field profile of the fundamental modes (a) HE_{11}^{x} and (b) HE_{11}^{y} near the phase matching.

Like many other fiber based SPR sensors, the proposed sensor operates very near to the phase matching point when there is coupling of the core guided mode to the surface plasmon wave propagating on the metal surface. Magnetic field profiles showing the surface plasmons is featured in Figure 4-3 (inserts (a) and (b)) with high losses being registered as a result of electromagnetic energy transfer to the surface plasmon.

Figure 4-4 also features the dispersion relationship between the core-guided mode (solid curves) and plasmon mode (dashed curves). It shows the phase matching points of the core-guided mode and the plasmon for both x and y polarizations. The x-polarized fundamental core guided mode (HE_{11}^{x}) crosses the x-polarized plasmon wave (plasmon x) at approximately 604nm whiles the y polarized fundamental core guided mode (HE_{11}^{y}) crosses the y-polarized plasmon wave (plasmon y) at approximately 624nm. At these points, the difference between the refractive indices of a pair (plasmon and fundamental) is the least.

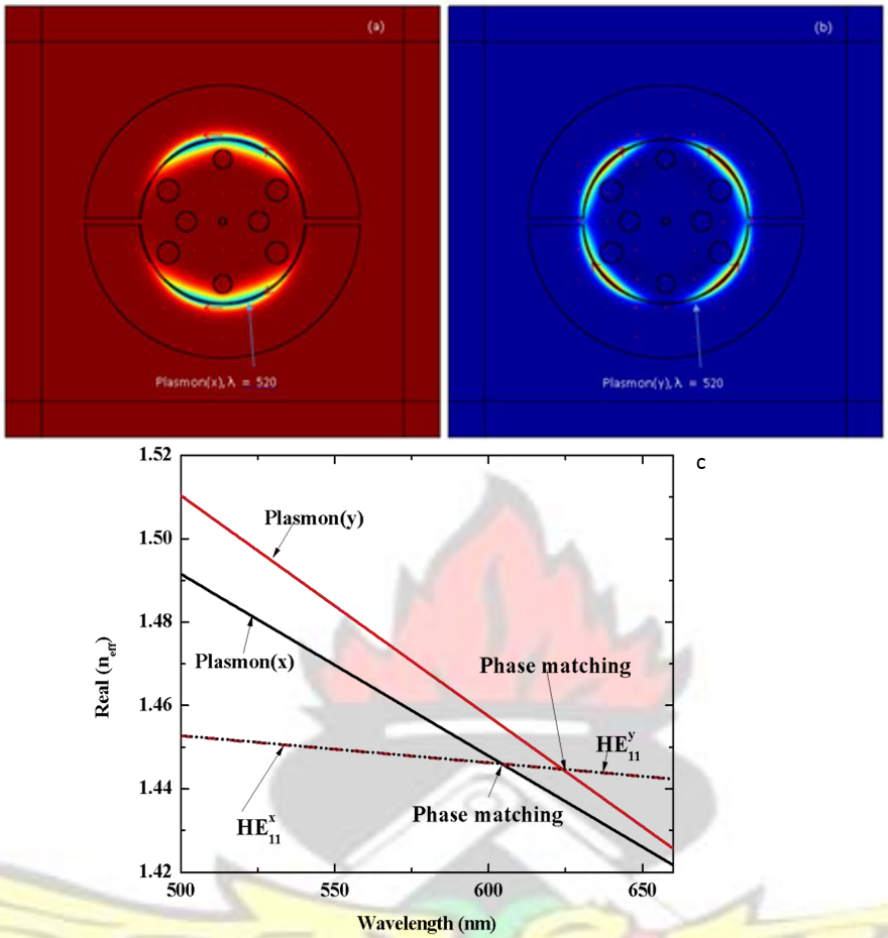

Figure 4-4 Dispersion relations of core-guided modes and surface plasmon(thick curve) in the vicinity of the phase matching point for the first plasmonic peak, (a) and (b) Magnetic field profile of plasmon modes.

Another compelling proof for the knowledge that there is coupling between the fundamental and plasmon modes at the phase matching point is featured in Figure 4-5.

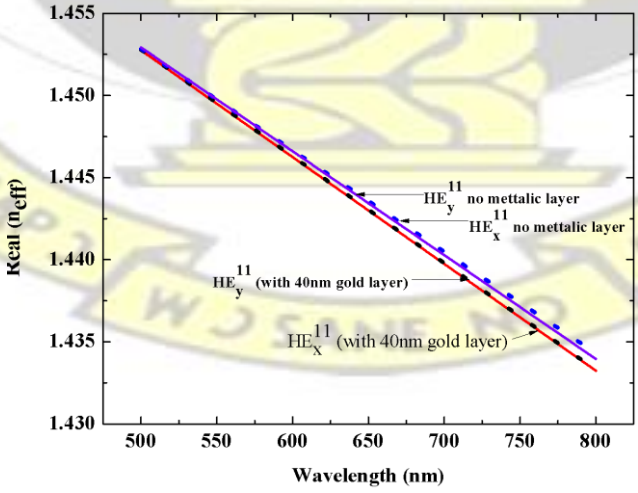

Figure 4-5 Comparison of the dispersion relations of core-guided modes of the proposed PCF SPR sensor with and without a metallic layer in the microfluidic slots

It displays the dispersion relationship of the proposed plasmon sensor with and without a metallic layer. It is easily observed that the effective indices of the fundamental modes for the two scenarios are very close to each other [142].

The presence of more than one peak in the loss spectra in some cases as compared to single peak loss spectrum is as a result of the significant effect the shape of the metal layer in the microfluidic slots. In other words, planar metallized surfaces support one peak in contrast to cylindrical metal surfaces that can support many plasmon peaks [[116]

The solid curve peaks and the dash curve peaks in Figure 4-2 correspond to the phase matching points of the core-guided mode to the plasmon mode with an analyte refractive index of 1.33 and 1.34 respectively. This transduction mechanism is used often for determining changes in the analyte bulk refractive index and also monitoring nanometer thin bio layer buildup on the metallized surface.

Surface plasmon waves propagate along the metallized surface. Therefore the thickness of the metal layer would affect the intensity of the surface excitations hence the sensitivity of the plasmon mode. To ascertain this fact, the analyte refractive index is fixed at 1.33 with all other structural parameters kept constant whiles the gold layer thickness was varied from 40nm to 50nm to observe the changes in loss spectra of the fundamental modes HE_{11}^{x} and HE_{11}^{y}. The results are plotted in Figure 4-6.

It is observed from Figure 4-6 that there is a decrease in modal propagation loss as the thickness of the gold layer is varied from 40nm to 50.

Additionally, the resonant peak at the phase matching point shifts to higher wavelengths, the relationship between sensitivity and metal layer thickness can be used in the study of metal nanoparticle binding events on the metallic surface of the sensor. A more practical approach would be its use in the monitoring of metal nanoparticle concentrations attached to the photosensitive drugs in photodynamic cancer therapy [116]

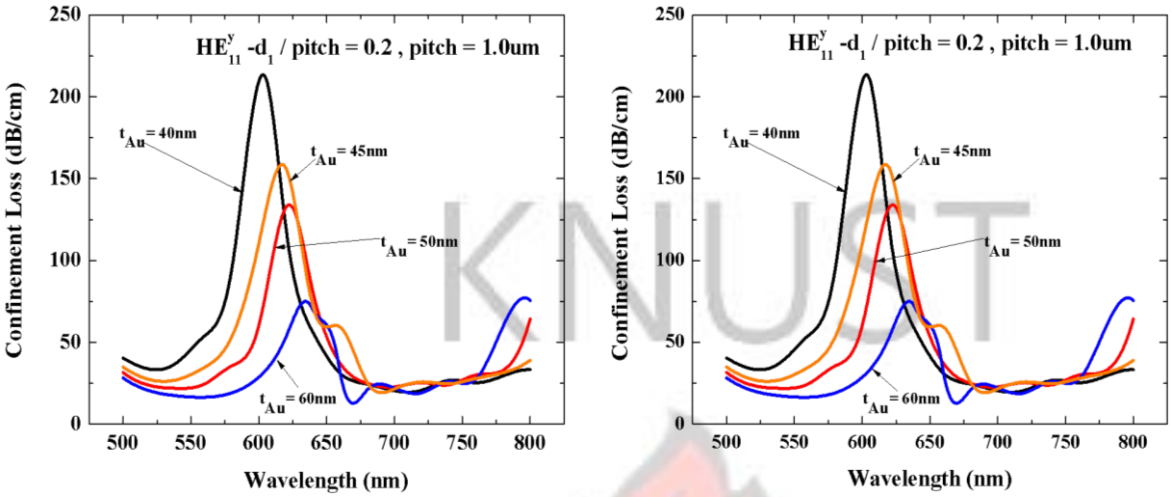

Figure 4-6 Loss spectra of proposed PCF SPR bio sensor in the vicinity of the plasmonic peak for variation in gold layer thickness (t_{Au}). Analyte refractive index (n_a =1.33)

Tuning to the phase matching point, is achieved by varying the structural parameter of the central air hole d_1. For the proposed model, d/Λ is varied from 0.20 to 0.30 with all other structural parameters kept constant. The microfluidic channels are filled with analyte with a refractive index, n_{ana} 1.33 the loss spectra is calculated for each varying value of d/Λ and the results plotted in Figure 4-7.

Figure 4-7 features a general increase in the modal losses of the two fundamental modes (HE_{11}^x and HE_{11}^y) as d_1/Λ is varied from 0.20 to 0.30. The increasing modal losses is as a result of the core guided mode being pushed outwards by the increasing diameter of the central air hole, d_1, thereby increasing its modal presence near the metallic surface resulting in higher propagation losses.

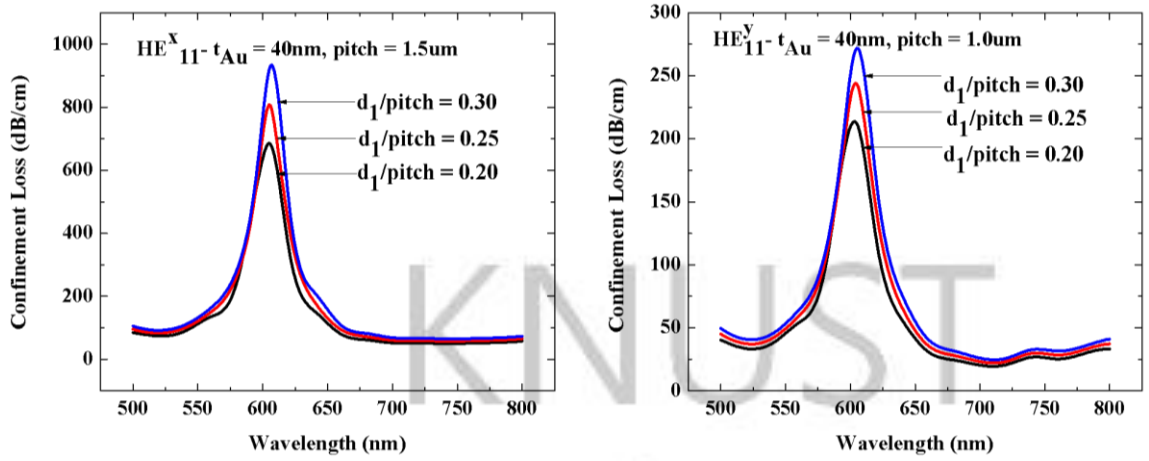

Figure 4-7 Loss spectra of proposed PCF SPR bio sensor in the vicinity of the plasmonic peak for variation in d1.

Furthermore, it can be observed that the modal refractive index reduces, as shown in Figure 4-8, as the core guided mode is pushed out from the central core region towards the metallized surface resulting in the shift of the plasmon peaks towards longer wave lengths (Figure 4-6).

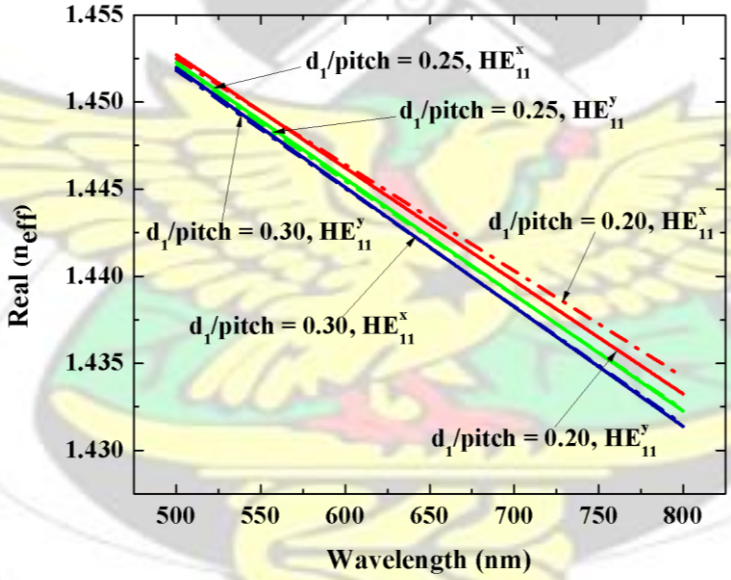

Figure 4-8 Dispersion relation of fundamental core-guided modes for variation in d_1.

4.3.1 Characterization of Sensor Sensitivity

The operations of most SPR sensors is based on the detection of change in the bulk refractive of the analyte[24, 116, 143]. The analyte refractive index has a strong dependence on the real part of the complex refractive index of the plasmon wave. This makes coupling between the core-guided mode and the plasmon mode at phase matching point very sensitive to changes in the analyte refractive index [24, 116]. There are two interrogation detection

methods used in this thesis;; amplitude or intensity interrogation and wavelength or spectral interrogation. With amplitude interrogation, sensitivity measurements are taken at a single wavelength which makes this interrogation technique very low cost and simple since there is no need for spectral manipulation.

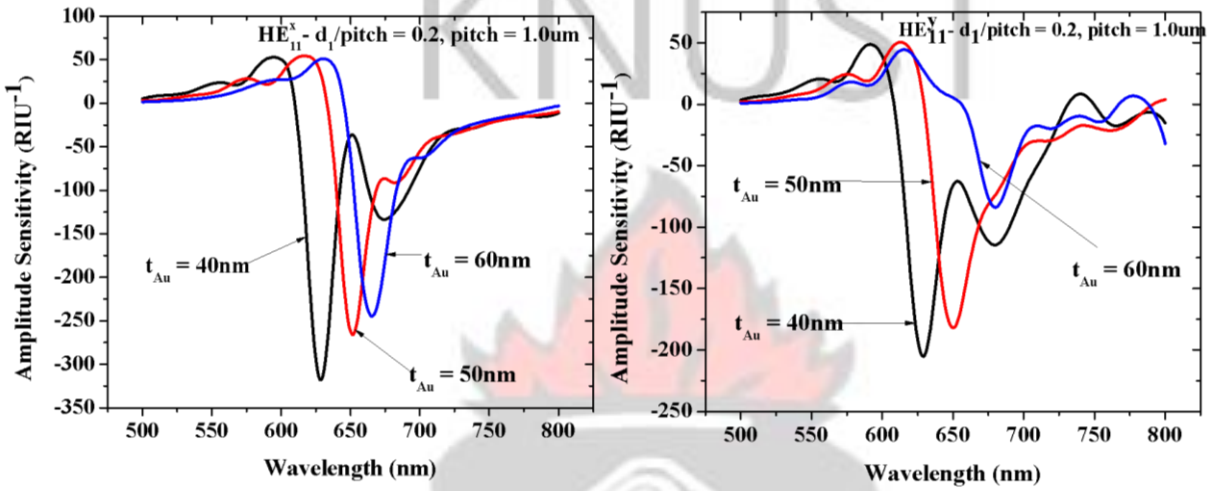

Figure 4-9 Variation of the amplitude sensitivity of the proposed PCF sensor for different thickness of gold.

The demerit however, is in its narrow operation range and lower sensitivity as compared to spectral interrogation technique in which spectra are compared every time the analyte refractive index changes [24, 116]. Amplitude sensitivity is given by [116].

$$S_A = \frac{\partial \alpha(\lambda, n_a)}{\partial n_a} \Big/ \alpha(\lambda, n_a) \quad \text{RIU}^{-1} \qquad (4.1)$$

where $\alpha(\lambda, n_a)$ is the propagation loss of the core mode as a function of wavelength.

Figure 4-9 illustrates the amplitude sensitivity of the proposed sensor for varying thickness of gold. The maximum sensitivity, from Figure 4-9, is 317.785 RIU^{-1} for the HE_{11}^x fundamental when t_{Au} = 40nm. As opposed to 205.2325 RIU^{-1}being recorded as the

maximum sensitivity for HE_{11}^{y} fundamental mode when t_{Au} = 40nm. Sensor resolutions of

3.147 10^{-5}RIU and

4.873 10^{-5}RIU for HE_{11}^{x} and HE_{11}^{y} respectively are attained if it is assumed that a change of

0.01 change in the transmitted intensity can be detected reliably.
In addition, it can be seen from Figure 4-9 that as t_{Au} increases, amplitude sensitivity decreases.

This is attributed to the fact that as the gold layer thickness increases the core-guided mode is

effectively screened from the plasmon mode weakening the coupling energy between the two.

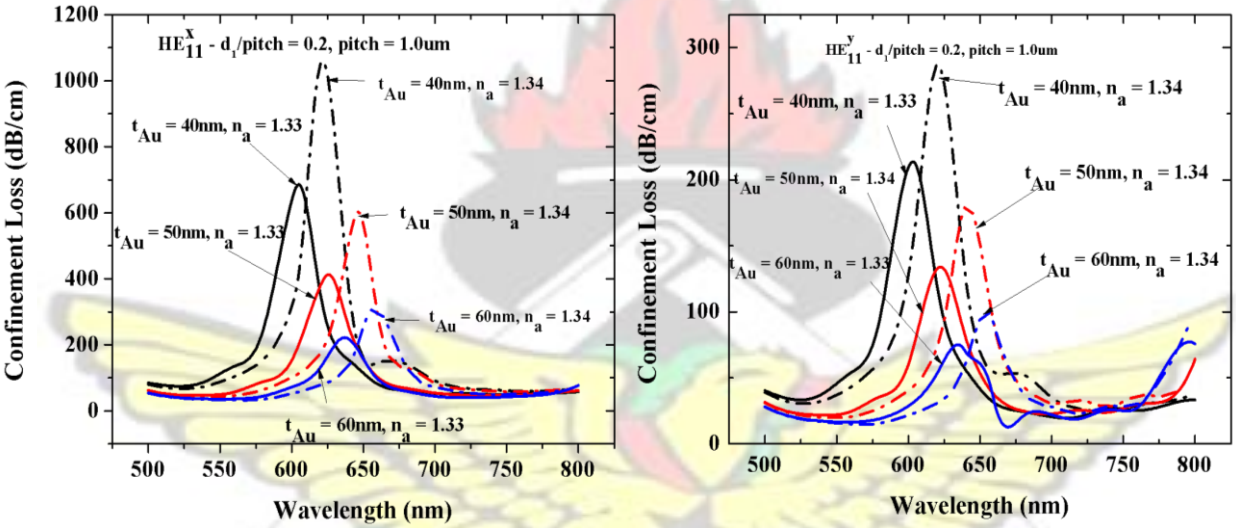

Figure 4-10 Variation in the shift of the resonant wavelength of the proposed PCF sensor for different thicknesses of gold.

Wavelength interrogation measurements are obtained by measuring the displacement of the plasmon peaks when the analyte refractive index is changed. Wavelength interrogation is mathematically expressed as:

$$S_{\lambda} = \frac{\Delta \lambda_{peak}}{\Delta n_a} \text{ nm/ RIU} \qquad 4.2$$

where λ_{peak} is the wavelength of the plasmonic peak at resonance condition. Shift in the plasmonic peaks of plots for loss spectra when t_{Au} is varied is illustrated in Figure 4-10. The

maximum λ_{peak} for HE_{11}^{x} mode is 17nm when t_{Au} 40nm whiles for HE_{11}^{y}, maximum λ_{peak} is 18nm when t_{Au} 40*nm*. Sensitivities of 1700nm/RIU and 1800nm/RIU are obtained for HE_{11}^{x} and HE_{11}^{y} respectively resulting in typical resolutions of 5.882 10^{-5}RIU and 5.556 10^{-5}RIUfor HE_{11}^{x} and HE_{11}^{y} respectively given a 0.01 change in refractive index.

To investigate the effect of birefringence on the spectral sensitivity, the parameter d_m/λ is varied from 0.40µm to 0.6µm without varying any of the other structural parameters. loss spectra for all variations of d_m/λ are plotted along with the birefringence values at resonance peaks for both fundamental modes (HE_{11}^{x} andHE_{11}^{y}) Figure 4-11 illustrates a general decrease in birefringence as d_m/λ increases and resonant peaks shifting towards shorter wavelength. There is also a general decrease in the modal losses of the two fundamental modes (HE_{11}^{x} and HE_{11}^{y}). This is as a result of the core guided mode being confined more to the core of the PCF.

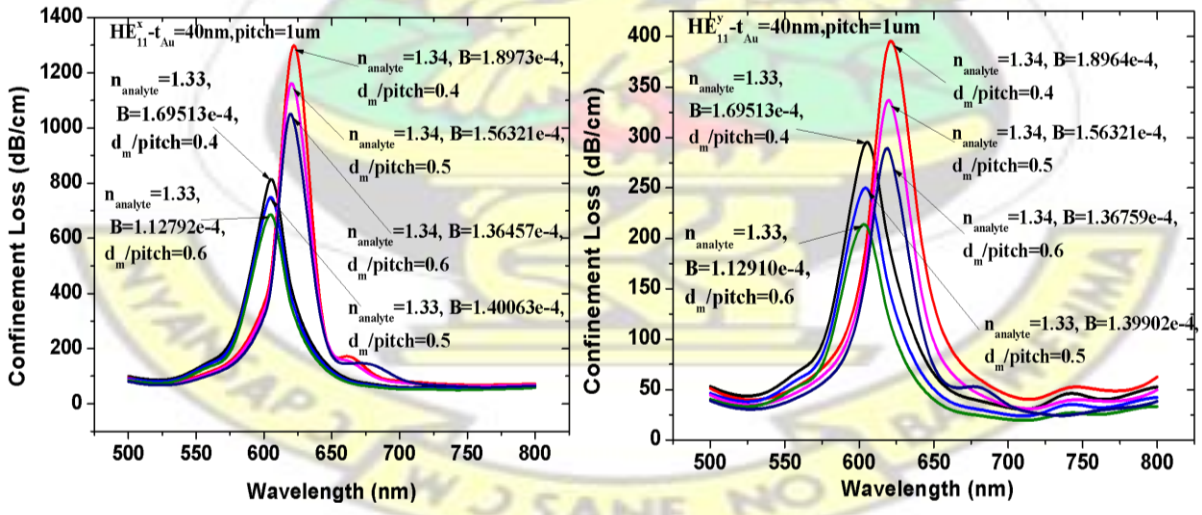

Figure 4-11 Loss spectra of proposed PCF SPR bio sensor in the vicinity of the plasmonic peak for variation in d3.

Figure 4-11 also features a general decrease of spectral sensitivity as birefringence decreases resulting in the shifting of resonance peaks to shorter wavelengths for both fundamental modes (

HE_{11}^{x} and HE_{11}^{x}). At d_m / □□ 0.20 the maximum □$_{peak}$ for HE_{11}^{x} mode is 17nm with a birefringence of 1.6953×10^{-4} and 1.8973×10^{-4} calculated at the phase matching point for n_a □1.33 and n_a □1.34 respectively. Whiles the maximum □$_{peak}$ for HE_{11}^{y} mode is 16 nm with a birefringence of. 1.69503□$10^{□4}$ and 1.8964□$10^{□4}$ calculated at the phase matching point for n_a □1.33 and n_a □1.34 respectively. Furthermore, at d_m / □□ 0.30 the maximum □$_{peak}$ for HE_{11}^{x} mode is 15nm with a birefringence of 1.12792□$10^{□4}$ and 1.36457□$10^{□4}$ calculated at the phase matching point for n_a □1.33 and n_a □1.34 respectively. Whiles the maximum □$_{peak}$ for HE_{11}^{y} mode at d_m / □□ 0.30 is 15nm with a birefringence of 1.1291□$10^{□4}$and 1.36759□$10^{□4}$ calculated at the phase matching point for n_a □1.33 and n_a □1.34 respectively.

Reducing losses at the plasmonic peaks can be achieved by modifying the structural properties (tuning) such as optimizing t_{Au} and d_1. However, sensitivity varies directly with losses therefore there should be a tradeoff between the two to ensure a balance between them.

It has been validated that this PCF design structure has the potential to support different sensitivities with respect to the two fundamental modes (HE_{11}^{x} and HE_{11}^{y}). It is possible to adjust the structural parameter d_1 and d_m to have substantial difference in the sensitivities with respect

to HE_{11}^{x} and HE_{11}^{y}. Exploitation of the birefringence for sensing has been successfully investigated in the next section for sensing multiple analytes aided by and metal oxide over layer to yield better sensitivity performance.

4.4 Multi Channel Bio sensor Design and Structural Characterisation

The schematic of the novel multi-channel photonic crystal fiber surface plasmon resonance bio sensor for multi-analyte sensing is illustrated in Figure 4-12(a).

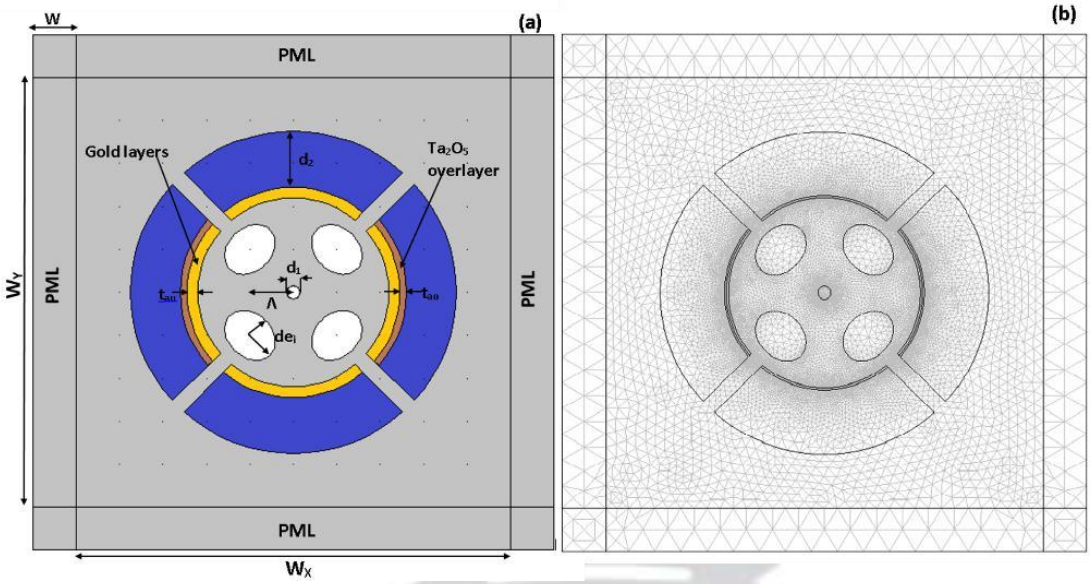

Figure 4-12 (a) Schematic of bio sensor showing various components.(b)Meshed module for numerical computation.

It comprises four micro fluid channels, d_2, with a gold layer of thickness t_{au}, on their inner sides. Additionally, a thin high refractive index di-electric over layer, tantalum pent-oxide ($Ta\ O_{2\ 5}$), of thickness t_{ao}, is applied on the gold layer in only two channels. The material properties of tantalum pent oxide layer is modelled from[76]

$$n_{Ta\ o^{2\ 5}} \square 1.878\ 178.4\ 10\square\square^{\ 2}/\square^{2}\ \square 52.7\ 10\square^{\ 7}/\square^{4} \qquad 4.3$$

Again, λ is the wavelength in nm.

Furthermore, four elliptical air holes, de_i (i denotes the minor or major axis), that form a low refractive index region for wave guidance and a central air hole, d_1, to tune resonance wave length of the guided mode to match that of the plasmon mode. The effective refractive index of air, n_{eff}, is 1.00. Also the analyte refractive index is denoted as n_{a1} for the horizontal micro fluidic slot pair (Channel 1) and n_{a2} for the vertical micro fluidic slot pair (Channel 2). The hole to hole spacing, Λ, as 1.0μm. Figure 4-12(b) shows the FEM meshed module and consist of 32404 elements with 226997 degrees of freedom. Anisotropic PML is also employed as the

boundary condition employed in the study of leaky modes as they travel through the fibre. Modal analysis is performed on the polarised fundamental modes, HE_{11}^{x} and HE_{11}^{y} in the x-y Cartesian plane as the mode propagates in the z direction.

The Multi channel bio sensor design is modelled using the following parameters; $\Lambda = 1.0\mu m$, $d_1/\Lambda = 0.30$, $d_2/\Lambda = 1.55$, $de_x/\Lambda = 0.65$, $de_y/\Lambda = 0.50$, $t_{au} = 50nm$, $t_{ao} = 40nm$. Channel 1 and Channel 2 are filled with an aqueous analyte of refractive index, $n_{a1}=1.33$ and $n_{a2} = 1.34$ respectively. Loss spectra and dispersion values for the two polarized modes, HE_{11}^{x} and HE_{11}^{y} are solved for over 400nm window.

4.4.1 Analysis of Structural and Performance Characterisation

Figure 4-13 illustrates the loss curve and dispersion relationship between the core guided mode and the plasmon mode at the phase matching wavelengths for x-polarized and ypolarized fundamental modes. The peaks in the loss curve (thick solid curve) indicate high energy losses of the core mode coupled to the plasmon.

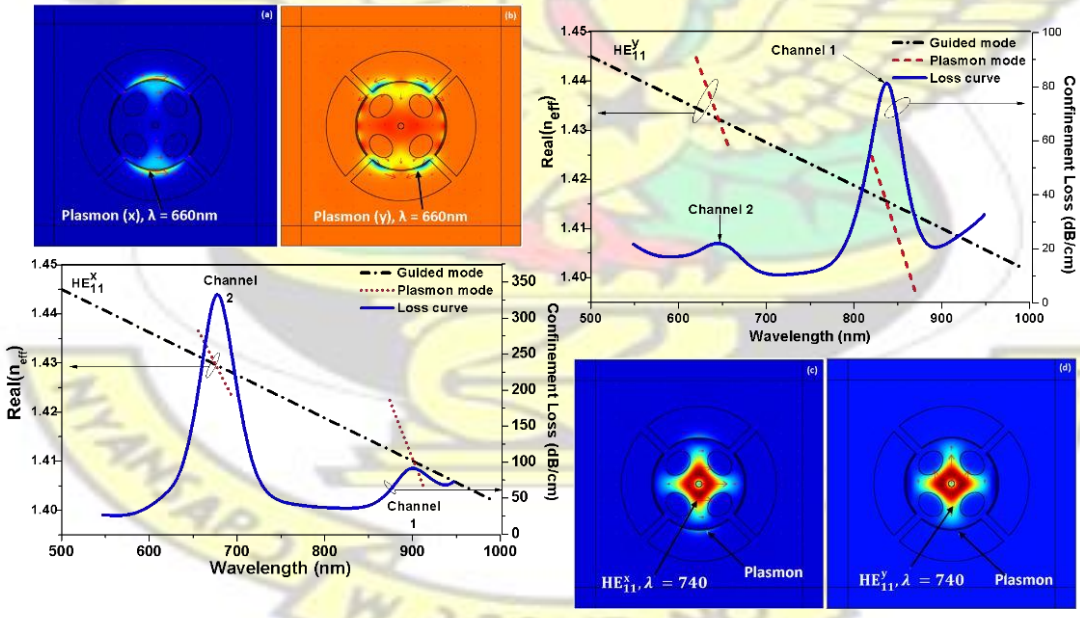

Figure 4-13 Loss curve and dispersion relationship between the core guided mode and the plasmon modes at resonant wavelength. For x-polarized and y-polarized fundamental modes. (a) and (b) are magnetic field distributions of plasmon mode.(c)and(d) are magnetic field

At these wavelengths, the two modes couple to one another because they have nearly equal effective refractive indices and propagation constants hence the core mode couples and resonates with the plasmon mode. The phase matching wavelengths are indicated by the intersection of the plasmon mode dispersion curve (dotted line) and core mode dispersion curve (dash-dot line) located around 675nm and 900nm for the x-polarized fundamental. While the y-polarized fundamental couples with the plasmon wave at 645nm and 836nm. Figure 4-13 also features magnetic field profiles of plasmon waves on the surface of the metal for both the x and y polarized fundamental modes (inserts (a) and (b)). This explains the high losses registered at those wavelengths. Fundamental modes exhibit different degrees of the core guided mode leaking to the plasmon mode. This depends on which mode has closer interaction with the plasmon. Inserts (c) and (d) illustrates the magnetic field distributions of the two fundamentally polarized modes, HE_{11}^{x} and HE_{11}^{y}, close to the phase matching wavelength. It is worthy to note that there is more leakage in the x-polarized fundamental as compared to the y-polarized fundamental.

Furthermore, Figure 4-14 features dispersion plots of the sensor with and without a metallized surface to support the plasmon for both x and y polarized fundamentals. It is easily observed that the effective indices of the fundamental polarized modes for both setups are in close proximity which is crucial for coupling of the core guided mode to the plasmon mode at resonance[142]

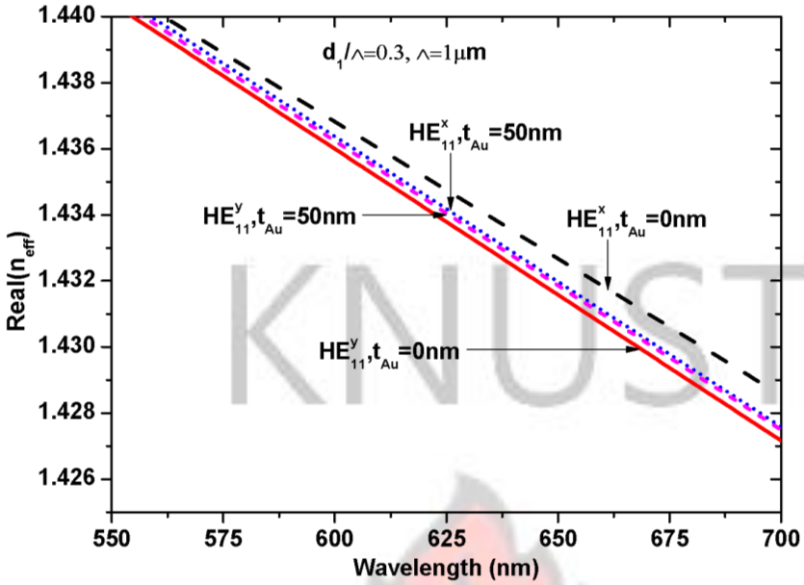

Figure 4-14 Dispersion relationship of fundamental mode with and without a layer of metal

4.5 Analysis of Bio sensor in Multiple Analyte Sensing mode

We go on to investigate the potential of the bio sensor for multi analyte sensing. In a first run, Channel 1 and Channel 2 are filled with aqueous analytes of refractive indices, n_{a1} = 1.33 and n_{a2} = 1.34 respectively whilst maintaining the same structural parameters as previously used. The second run is made with different set of refractive indices, n_{a1} = 1.34, and n_{a2} = 1.35. The confinement loses of both polarized modes (HE_{11}^{x} and HE_{11}^{y}) are obtained for each run. Figure 4-15 illustrates the results obtained from the two runs, in the form of spectra loss plots for HE_{11}^{x} and HE_{11}^{y} modes.

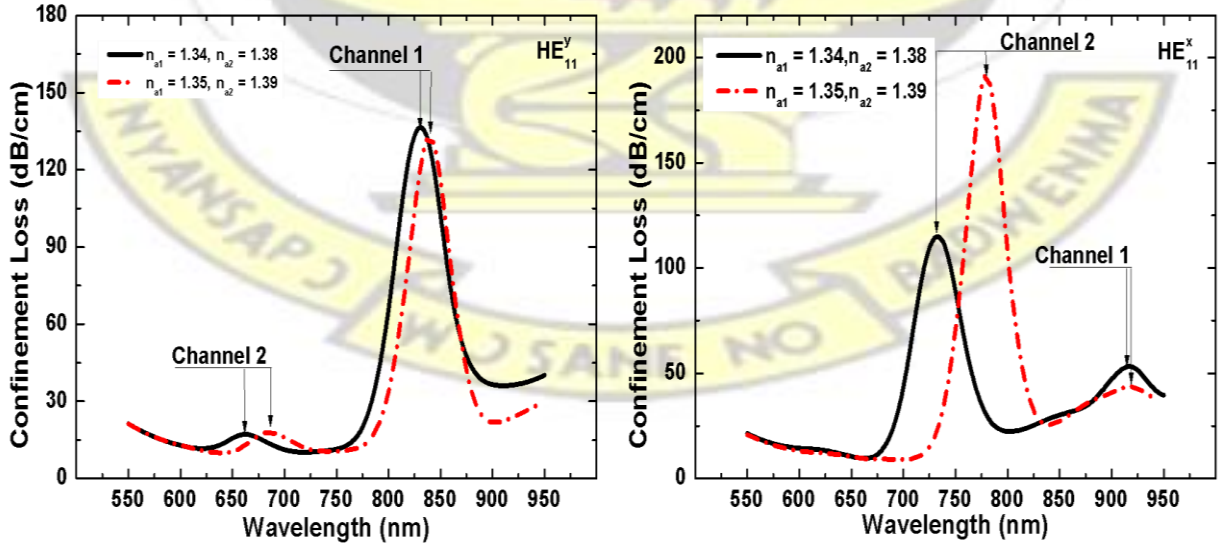

Figure 4-15 Dual analyte operation of bio sensor showing loss spectra of x and y polarizations of the fundamental modes (HE_{11}^{x} and HE_{11}^{y}). Attenuation peaks correspond to excited plasmons on the gold surface. The change of line type correspond to change in analytes in both.

Two peaks are observed to occur in the loss curves. The coupling of the core guided mode to the plasmon mode occurs at two resonance wavelengths because of the presence of two different analytes. The shift in the loss curves for each polarized fundamental mode is attributed to the change in the analyte refractive used in both runs. As the surface plasmon is sensitive to changes in the analyte refractive index, the phase matching points vary as such.

The bulk and surface refractive index change can be monitored using this method.

4.6 Bio sensor Analysis in Self -Referencing Mode

To ascertain the potential of the metallized bio sensor to operate in self-referencing mode, n_{a1} is fixed at 1.33 in Channel 1 while n_{a2} is varied from 1.32 to 1.36 in Channel 2 without altering any other structural parameters. As can be seen from Figure 4-14, the variation of the analyte refractive index in Channel 2 causes the peaks to shift towards longer wavelengths while the no shifts are detected for Channel 1 containing the fixed analyte. This happens for both HE_{11}^{x} and HE_{11}^{y} modes. The distinguishing feature is the change of the much lossy Channel 2 of the HE_{11}^{x} mode to the Channel 1 in HE_{11}^{y}. This is attributed to stronger coupling of HE_{11}^{x} mode to plasmon mode in Channel 2 than Channel 1 whilst HE_{11}^{y} couples better with the plasmon in Channel 1 than Channel 2.

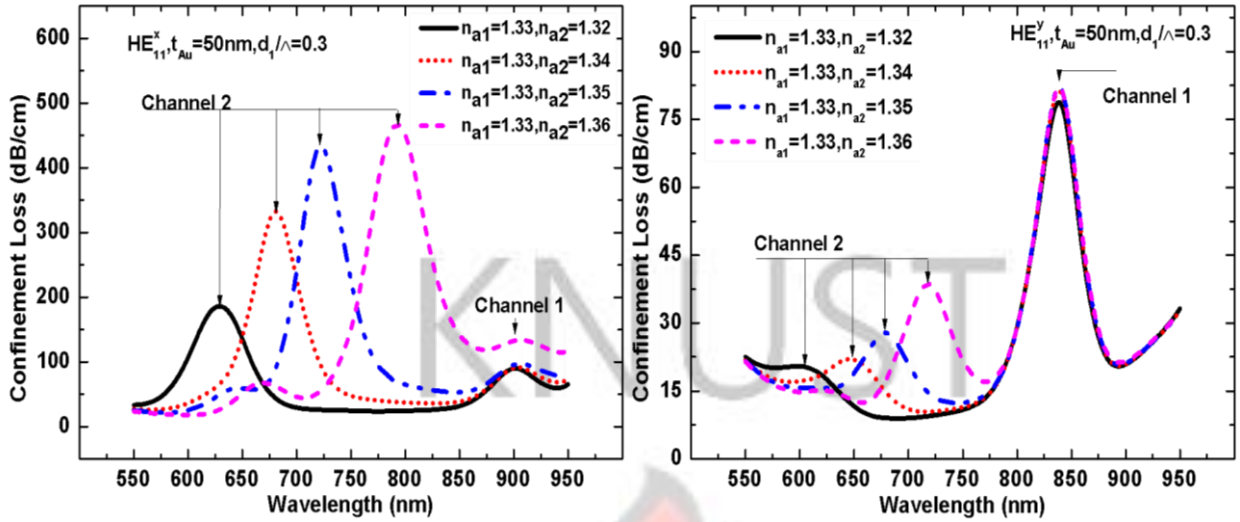

Figure 4-16 Self-referencing operation of bio sensor showing loss spectra of x and y polarizations of the fundamental modes (HE_{11}^{x} and HE_{11}^{y})

4.6.1 Influences of Structural Parameters

This photonic crystal fiber bio sensor is very sensitive to changes in its structural variables enabling its operation to be optimized by way of fine tuning. This section expounds on the influences of four structural variables, namely, the central air hole, d_1/Λ, the elliptical cladding air hole, de_i/Λ, thickness of gold layer, t_{au}, and over layer thickness, t_{ao}. With each investigation of the effect of a structural variable, all other structural variables remain as they were first defined.

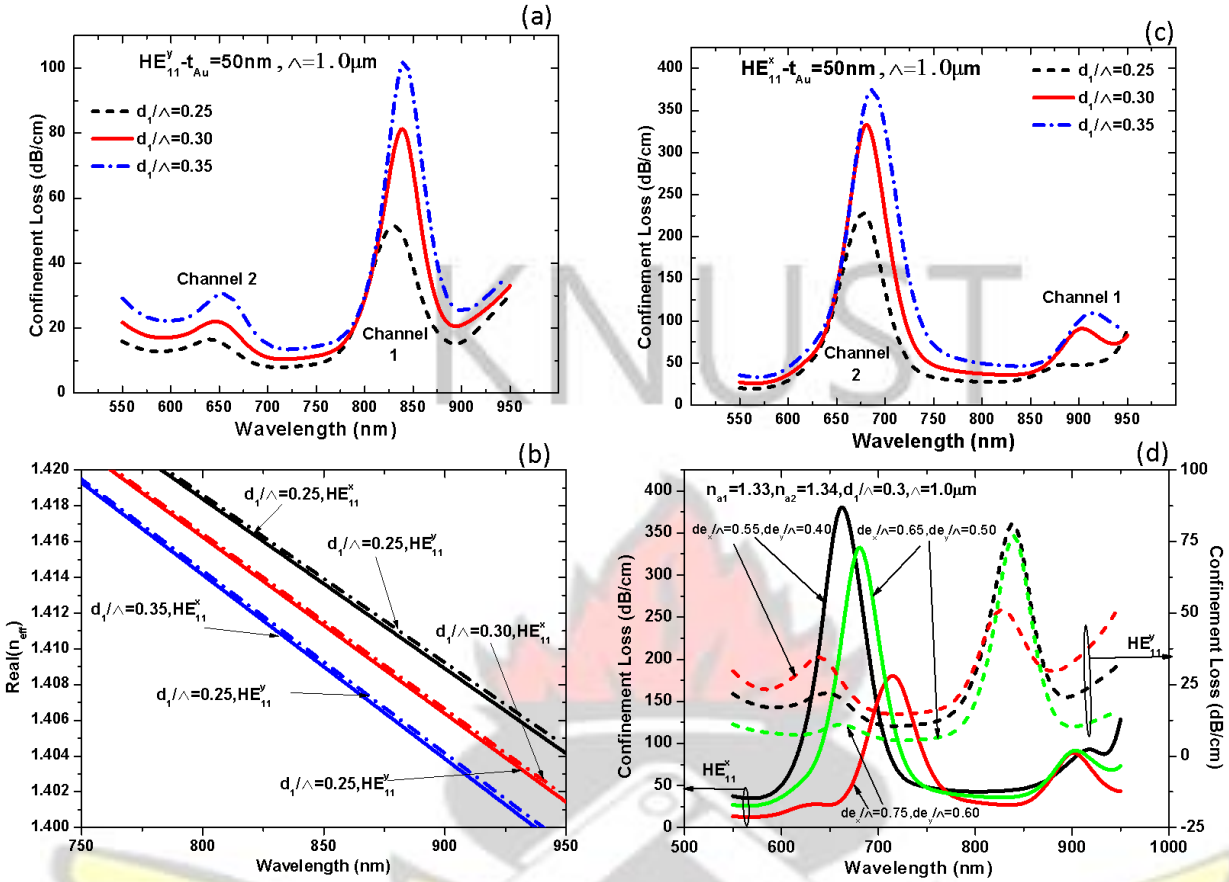

Figure 4-17 Dependence of resonance peak wavelength on central air hole for HE_{11}^{x} and HE_{11}^{x} (inserts (a) and (c)). Insert (b) displays dispersion trend for varying central air hole for and .Result on display are for the bio sensor operating in self-referencing mode

The core guided mode is pushed outwards and its presence increases near the metal layer as d_1/Λ is varied from 0.25 to 0.35 resulting in increasing mode loss to the surface plasmon and shifting of the resonance peaks to longer wavelengths. Figure 4-17a figure 4-17b elucidates the effects of d_1/Λ on mode loss for$_{HE_{11}^{x}}$and$_{HE_{11}^{y}}$. In addition, the dispersion plots, figure 4-17c show a general decrease in the refractive indices.

Furthermore, the core guided mode is effectively shielded and its presence decreases near the metal layer as de_x/Λ and de_y/Λ is varied from 0.55 to 0.75 and 0.40 to 0.60 respectively resulting in decreasing mode loss (channel 2) to the surface plasmon and shifting of the resonance peaks to shorter wavelengths. Figure 6d elucidates the effects of de_x/Λ and de_y/Λ on mode loss.

Alluding to the fact that surface plasmon modes are metal surface phenomena, we can predict there being a relation between the two. We investigate this by varying t_{au} from 45nm to 55nm with channel 1 and channel 2 containing aqueous samples of refractive indices 1.33 and 1.34 respectively. Figure 4-18a and 4-18b shows the loss curves with peaks shifting to longer wavelengths in and decreasing guided mode losses (as guided mode is shielded more from plasmon) for each variation in t_{au} for channel 2 but an inverse for channel 1. The presence of a high refractive index over layer in channel 1 converts the shielding effect to a magnifying one inducing a stronger plasmon supported by the thickening gold layer hence stronger coupling and larger mode loss .Such a relation provides an opportunity for the study of metal surface particle activities at nano-scale level[116].

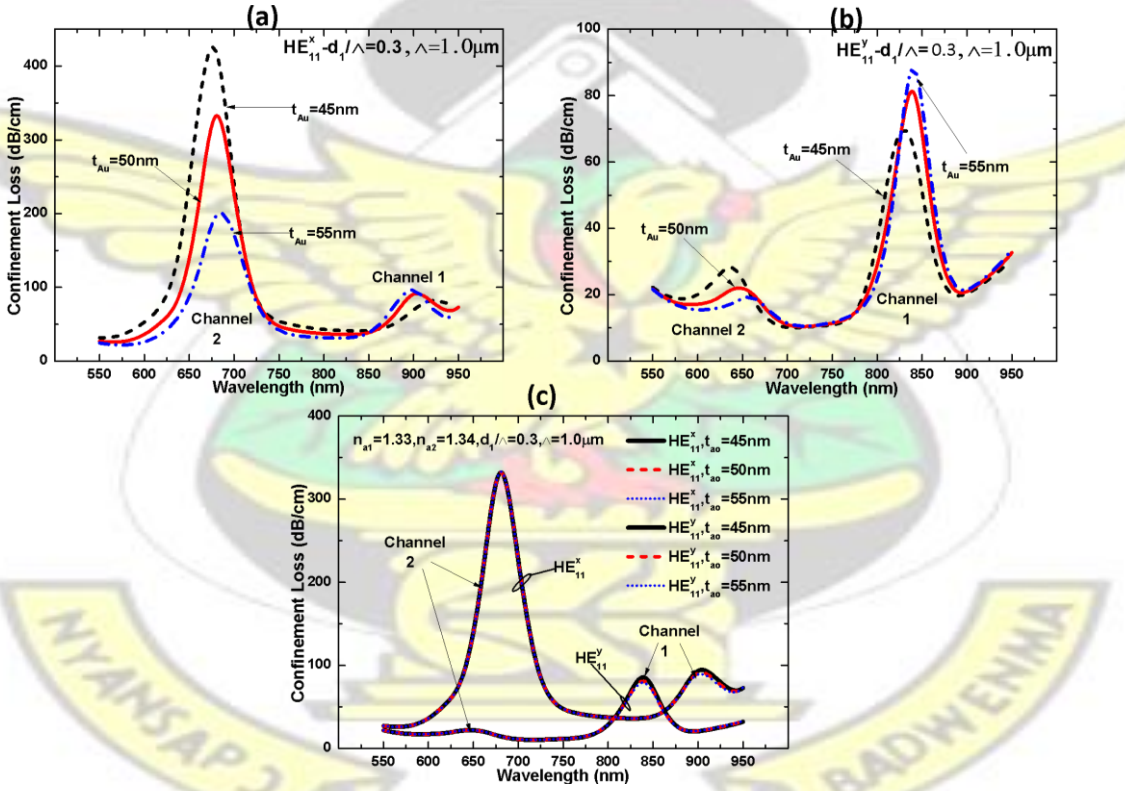

Figure 4-18 Effect of variation of gold thickness on loss for proposed PCF bio sensor operating in self-referencing mode(inserts (a) and (b)) for HE_{11}^{x} and HE_{11}^{y} modes. The dependence of loss spectra on overlay thickness is also displayed in insert (c).

We go further to study the effect of over layer thickness on modal loss as t_{ao} is varied from

20nm to 60nm. Figure 4-18c shows changes in modal loss of channel 1and with no plasmon peak shifts for both fundamental HE_{11}^{x} and HE_{11}^{y} modes. It shows a general decrease in modal loss in channel 1 as t_{ao} is varied.

4.6.2 Characterization of Sensor Sensitivity

The sturdy dependence of the surface plasmon wave on the analyte refractive index is the underlying principle used by most sensors to detect changes. The variation of the analyte refractive index causes an associated shift in the resonance wavelength. Both bulk and surface refractive index changes contribute to the shift of the resonance wavelength. Analysis of the resonant wavelength shifts can be done in two ways; intensity or amplitude interrogation and wavelength or spectral interrogation. The degree of discrimination in wavelength or intensity determines how sensitive the sensor is.

Amplitude interrogation in comparison to wavelength interrogation is more economical and simple to implement [144]. However its low sensing capability and small range of operation make wavelength interrogation a better choice in that respect. Mathematically, amplitude sensitivity can be represented as

$$S(\ )_A = \frac{\partial((,n)/ n)/_a}{\partial_a \partial(,n_a)} [RIU^{-1}] \text{ per refractive index units} \quad 4.4$$

$\partial\ \partial$ $,n_a$ represents lost energy of the core mode as at a particular wavelength[25]. As illustrated in Figure 4-19, the bio sensor operating in self-referencing mode recorded typical sensing values of 425 RIU^{-1} and 131 RIU^{-1} for both HE_{11}^{x} and HE_{11}^{y} modes respectively with t_{au}=45nm This resolves to resolution values of 2×10^{-5} RIU and 7×10^{-5} RIU for x and y polarized fundamental modes in self-referencing mode assuming a reliable detection of 1% change in intensity is made in both modes.

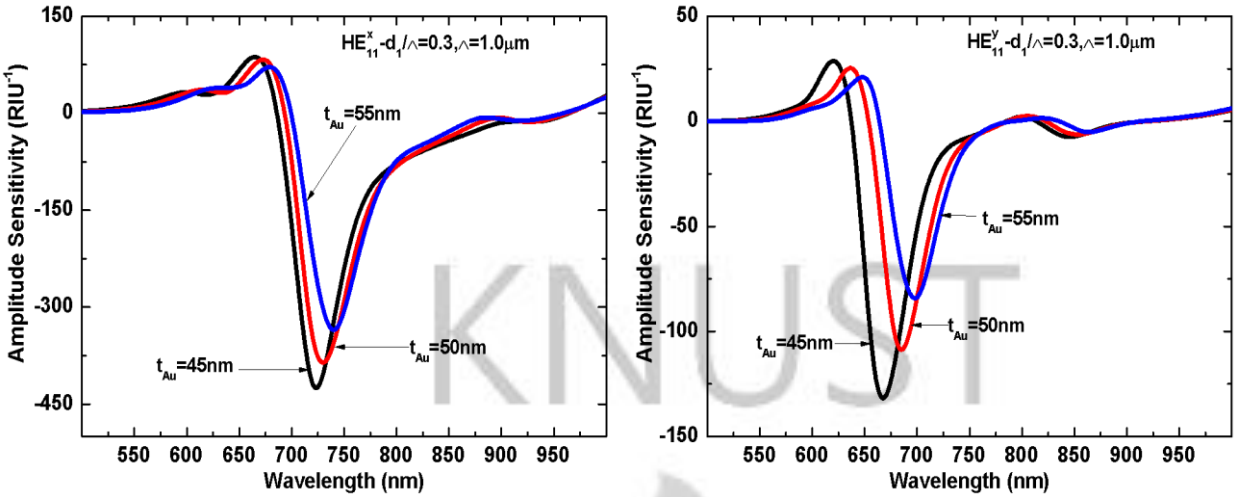

Figure 4-19 Relationship between amplitude sensitivity and gold layer thickness of the PCF bio sensor for varying $t_{Au.}$

Furthermore, one can notice from Figure 4-19 that amplitude sensitivity is inversely related to t_{au}. This is because as the gold layer thickens, it blocks more of the leakage of the core guided mode to the plasmon mode weakening the coupling between the two resulting in lower sensitivities. The stronger presence of the x polarized fundamental mode near the gold layer is responsible for the higher sensitivity value for it as compared to the y polarized mode at t_{au} = 45nm.

Moving on, wavelength interrogation is applied to the bio sensor operating in both multianalyte and self-referencing modes to characterize its sensing capability. Spectral interrogation is define mathematically as

$$S(\lambda) = \frac{\Delta\lambda_{peak}}{\Delta n_a} \text{ [nm / RIU]} \qquad 4.5$$

$\Delta\lambda_{peak}$is the wavelength at which the loss peaks occur. The bio sensor operating in multianalyte mode has the largest$\Delta\Delta\lambda_{peak}$ of 46nm (Channel 2) and 23nm (Channel 1) forHE_{11}^{x} and HE_{11}^{y} occurring when t_{au}=50nm resulting in spectral sensitivities of 4600nm/RIU and 2300nm/RIU respectively. Assuming a reliable detection of 0.1nm change in the resonance

position, typical sensor resolutions of 2×10^{-5}RIU and 4×10^{-5}RIU are made in both modes respectively. Considering the bio sensor operating in self-referencing mode, maximum$\square\square_{peak}$ values of 41nm (Channel 2) and 33nm (Channel 2) are recorded for HE_{11}^{x} and HE_{11}^{y} occurring when t_{au}=50nm resulting in spectral sensitivities of 4100nm/RIU and 3300nm/RIU respectively. Assuming a reliable detection of 0.1nm change in the resonance position, typical sensor resolutions of 2×10^{-5} RIU and 3×10^{-5} RIU are made in both modes respectively.

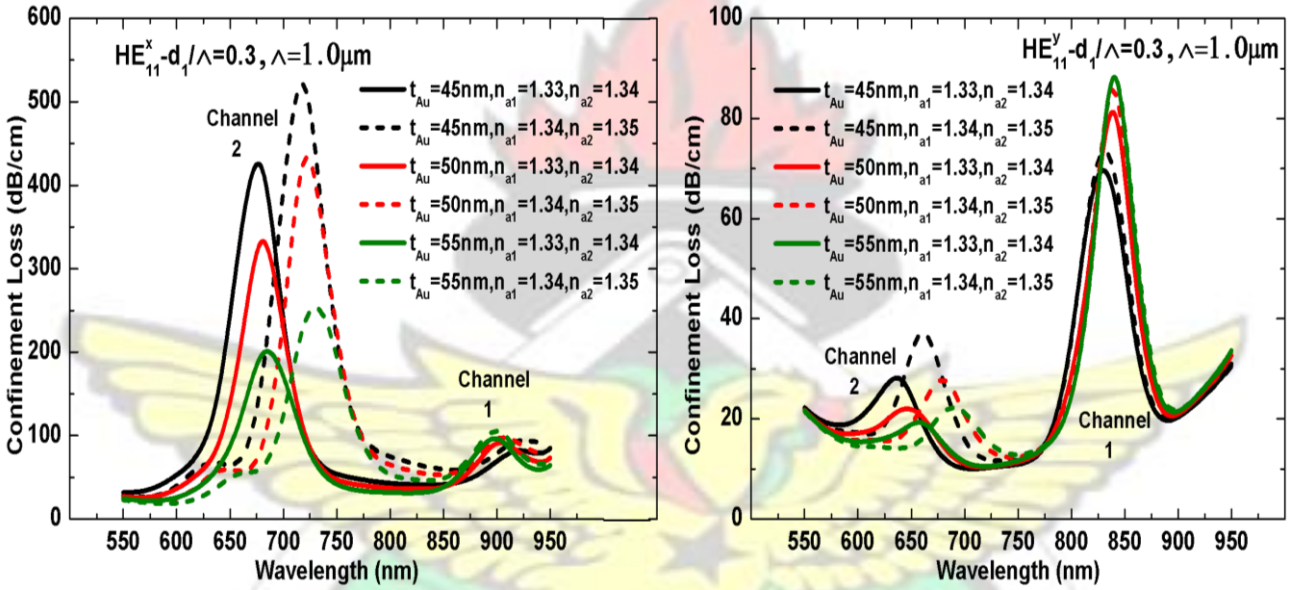

Figure 4-20 Resonant wavelength dependence on gold thickness and analyte refractive index.

Figure 4-18 shows the loss peaks and the wavelengths at which they occur as t_{au} is varied from 45nm to 55nm for both operational modes.

4.7 Fabrication

Fabrication of the two bio sensor should be relatively easy primarily due to the few but large holes especially in the dual channel design[145]. In addition, aqueous samples can be introduced into the slots either with pressure or capillary action [146-148]. High pressure chemical vapour technique is one efficient way to apply gold depositions on the inner surfaces of the micro fluidic slots [149]. Alternatively, electrolytic plating can be used to deposit the required amount of gold[144, 150].

CHAPTER 5: CONCLUSIONS AND RECOMMENDATIONS

5.1 Conclusion

This thesis presented a study about the use of photonic crystal fibers for label free optofluidic bio sensor applications based on surface plasmon resonance with considerable performance in refractive index sensitivity and resolution. With many significant advantages such as remote sensing capability, robustness, potential for integration with other components and portability make PCFs a very suitable fiber technology for SPR based sensing schemes.

A strong motivation for the PCF fiber technology is discussed in chapter 1 of this thesis. A detailed presesntation of the development of fiber sensing technolgy based on SPR and physics is in chapter 2 . chapter three explores the modelling of sinle and multi analyte sensing fibers and their numerical investigation thereof with FEM. The results obtained are discussed in chapter 4. The multi analyte sensor proposed in this thesis is to solve the problem of traditional single analyte sensors not able to distinguish between bulk and surface refractive index changes. In addition, other challenges such as temperature and noise that introduce errors into sensitivity and resoulution can be combated.

The use of birefringence for multi analyte sensing is introduced by the dual channel sensor and implemented by the elliptical air hole core guided PCF SPR sensor. The ellipical air hole bio sensor uses both long and short range surface plasmon modes to diffrentiate bulk and surface binding events.

Investigation performed on the single analyte sensor considered the sensor operating in both amplitude and wavelength interrogation modes and the effect of birefringence on performance parameters of the model. Characteristic sensor resolutions of 5.882 10 $^{-5}$*RIU* and 5.556 10

^{-5}RIU with respect to HE_{11}^{x} and HE_{11}^{y} respectively was reported for the wavelength interrogation mode, whilst 3.147 10 ^{-5}RIU and 4.873 10 ^{-5}RIU for HE_{11}^{x} and HE_{11}^{y} respectively for the amplitude interrogation mode. These estimated resolutions are comparable to reported designs in [119, 120]. Birefringence can be used to re-calibrate the phase matching point to shorter wavelengths with lower losses

Both single and multi analyte sensors have large sized air holes and fluidic channels that facilitate aqueous sample loading with pressure or capillary action and the fabrication of single and multiple layers respectively. The thin gold layer on the inner surfaces of the micro fluidic slots can be achieved using high pressure chemical vapour technique. Alternatively, electrolytic plating can be used to deposit the required amount of gold.

The multi analyte bio sensor can be reconfigured to operate in two modes; dual analyte sensing mode and in self-referencing mode. The operation of the bio sensor in dual analyte mode enables detection of two analytes in one aqueous sample. It can also be used in the identification of two different liquid samples each containing a different analyte. Similarly, self-referencing operation mode eliminates external influences (instrumental noises variation of non-target analytes, and temperature fluctuation).

The coupling conditions at resonance, sensitivity, and loss spectra of this SPR based PCF bio sensor has been investigated using a finite element method and perfectly matched layered boundaries. It has been validated that the PCF design structure can operate in two modes and measure different sensitivities for each fundamental mode (HE_{11}^{x} and HE_{11}^{y}). The bio sensor, in multi analyte operation, mode has characteristic sensor resolution values of 2×10^{-5} RIU and 4×10^{-5}RIU for HE_{11}^{x} and HE_{11}^{y} modes are recorded for the spectral interrogation mode. On the other hand, in self-referencing operational mode, characteristic sensor resolution values of

2×10^{-5}RIU and 3×10^{-5}RIU for HE_{11}^{x} and HE_{11}^{y} modes are recorded for the spectral interrogation mode whilst 2×10^{-5} RIU for HE_{11}^{x} mode and 7×10^{-5} RIU for HE_{11}^{y} modes when the amplitude interrogation mode is performed. The resolutions obtained are better in comparison to those reported designs in [337,338]

5.2 Future Work

It is recommended for future work for research to focus on noise reduction and sensitivity improvement. Further study on both the sensor design and the sensing experiment design would lead to possible break through. Also, further measurements of the surface properties of the sensor should be conducted because the sensor surface is a critical factor in sensing performance. It's been assumed in this thesis that non-specific binding only occurs in the analyte whereas specific binding occurs on the substrate surface. It is possible that the both binding events on the substrate.

REFRENCES

[1] S. Chen, *Miniaturized localized surface plasmon resonance biosensors*: Chalmers University of Technology, 2013.

[2] S. Kurosawa, M. Nakamura, J.-W. Park, H. Aizawa, K. Yamada, and M. Hirata, "Evaluation of a high-affinity QCM immunosensor using antibody fragmentation and 2-methacryloyloxyethyl phosphorylcholine (MPC) polymer," *Biosensors and Bioelectronics,* vol. 20, pp. 1134-1139, 2004.

[3] G. Wu, R. H. Datar, K. M. Hansen, T. Thundat, R. J. Cote, and A. Majumdar, "Bioassay of prostate-specific antigen (PSA) using microcantilevers," *Nature biotechnology,* vol. 19, pp. 856-860, 2001.

[4] J. H. Lee, K. S. Hwang, J. Park, K. H. Yoon, D. S. Yoon, and T. S. Kim, "Immunoassay of prostate-specific antigen (PSA) using resonant frequency shift of piezoelectric nanomechanical microcantilever," *Biosensors and Bioelectronics,* vol. 20, pp. 2157-2162, 2005.

[5] L. Liu, Y.-y. Chen, Y.-h. Meng, S. Chen, and G. Jin, "Improvement for sensitivity of biosensor with total internal reflection imaging ellipsometry (TIRIE)," *Thin Solid Films,* vol. 519, pp. 2758-2762, 2011.

[6] T. Neumann, H. Junker, K. Schmidt, and R. Sekul, "SPR-based fragment screening: advantages and applications," *Current topics in medicinal chemistry,* vol. 7, pp. 16301642, 2007.

[7] A. Guidi, L. Laricchia-Robbio, D. Gianfaldoni, R. Revoltella, and G. Del Bono, "Comparison of a conventional immunoassay (ELISA) with a surface plasmon resonance-based biosensor for IGF-1 detection in cows' milk," *Biosensors and Bioelectronics,* vol. 16, pp. 971-977, 2001.

[8] B. Liedberg, C. Nylander, and I. Lunström, "Surface plasmon resonance for gas detection and biosensing," *Sensors and actuators,* vol. 4, pp. 299-304, 1983.

[9] C. Nylander, B. Liedberg, and T. Lind, "Gas detection by means of surface plasmon resonance," *Sensors and Actuators,* vol. 3, pp. 79-88, 1983.

[10] J. Homola, H. Vaisocherová, J. Dostálek, and M. Piliarik, "Multi-analyte surface plasmon resonance biosensing," *Methods,* vol. 37, pp. 26-36, 2005.

[11] R. Schilling, "Self-Referencing and Sensitivity Optimization in Photonic Crystal Slabs for Biosensing Applications," University of Toronto, 2013.

[12] M. Baaske and F. Vollmer, "Optical resonator biosensors: molecular diagnostic and nanoparticle detection on an integrated platform," *ChemPhysChem,* vol. 13, pp. 427436, 2012.

[13] D. Erickson, S. Mandal, A. H. Yang, and B. Cordovez, "Nanobiosensors: optofluidic, electrical and mechanical approaches to biomolecular detection at the nanoscale," *Microfluidics and nanofluidics,* vol. 4, pp. 33-52, 2008.

[14] S. Peng and G. M. Morris, "Resonant scattering from two-dimensional gratings," *JOSA A,* vol. 13, pp. 993-1005, 1996.

[15] M. El Beheiry, V. Liu, S. Fan, and O. Levi, "Sensitivity enhancement in photonic crystal slab biosensors," *Optics express,* vol. 18, pp. 22702-22714, 2010.

[16] J. Zenneck, "Über die Fortpflanzung ebener elektromagnetischer Wellen längs einer ebenen Leiterfläche und ihre Beziehung zur drahtlosen Telegraphie," *Annalen der Physik,* vol. 328, pp. 846-866, 1907.

[17] A. Sommerfeld, "Propagation of waves in wireless telegraphy," *Ann. Phys,* vol. 28, pp. 665-736, 1909.

[18] R. Ritchie, "Plasma losses by fast electrons in thin films," *Physical Review,* vol. 106, p. 874, 1957.

[19] C. Powell and J. Swan, "Effect of oxidation on the characteristic loss spectra of aluminum and magnesium," *Physical Review,* vol. 118, p. 640, 1960.

[20] E. Stern and R. Ferrell, "Surface plasma oscillations of a degenerate electron gas," *Physical Review,* vol. 120, p. 130, 1960.

[21] A. Otto, "Excitation of nonradiative surface plasma waves in silver by the method of frustrated total reflection," *Zeitschrift für Physik,* vol. 216, pp. 398-410, 1968.

[22] E. Kretschmann and H. Raether, "Radiative decay of non radiative surface plasmons excited by light(Surface plasma waves excitation by light and decay into photons applied to nonradiative modes)," *Zeitschrift Fuer Naturforschung, Teil A,* vol. 23, p. 2135, 1968.

[23] B. Liedberg, C. Nylander, and I. Lundström, "Biosensing with surface plasmon resonance—how it all started," *Biosensors and Bioelectronics,* vol. 10, pp. i-ix, 1995.

[24] J. Homola, S. S. Yee, and G. Gauglitz, "Surface plasmon resonance sensors: review," *Sensors and Actuators B: Chemical,* vol. 54, pp. 3-15, 1999.

[25] R. Ince and R. Narayanaswamy, "Analysis of the performance of interferometry, surface plasmon resonance and luminescence as biosensors and chemosensors," *Analytica chimica acta,* vol. 569, pp. 1-20, 2006.

[26] P. V. Lambeck, "Integrated opto-chemical sensors," *Sensors and Actuators B: Chemical,* vol. 8, pp. 103-116, 1992.

[27] R. Guenther, "Modern Optics John Wiley & Sons," *New York,* p. 43, 1990.

[28] E. H. Hellen and D. Axelrod, "Fluorescence emission at dielectric and metal-film interfaces," *JOSA B*, vol. 4, pp. 337-350, 1987.

[29] S. Blair and Y. Chen, "Resonant-enhanced evanescent-wave fluorescence biosensing with cylindrical optical cavities," *Applied Optics*, vol. 40, pp. 570-582, 2001.

[30] J. Homola, "Surface plasmon resonance sensors for detection of chemical and biological species," *Chemical reviews*, vol. 108, pp. 462-493, 2008.

[31] J. Homola, "Present and future of surface plasmon resonance biosensors," *Analytical and bioanalytical chemistry*, vol. 377, pp. 528-539, 2003.

[32] A. K. Sharma, R. Jha, and B. Gupta, "Fiber-optic sensors based on surface plasmon resonance: a comprehensive review," *Sensors Journal, IEEE*, vol. 7, pp. 1118-1129, 2007.

[33] S. A. Maier, *Plasmonics: Fundamentals and Applications: Fundamentals and Applications*: Springer, 2007.

[34] G. Ruffato, "Plasmonic Gratings for Sensing Devices," 2012.

[35] M. Ordal, L. Long, R. Bell, S. Bell, R. Bell, R. Alexander Jr, and C. Ward, "Optical properties of the metals al, co, cu, au, fe, pb, ni, pd, pt, ag, ti, and w in the infrared and far infrared," *Applied Optics*, vol. 22, pp. 1099-1119, 1983.

[36] R. Alonso, F. Villuendas, J. Tornos, and J. Pelayo, "New 'in-line'optical-fibre sensor based on surface plasmon excitation," *Sensors and Actuators A: Physical*, vol. 37, pp. 187-192, 1993.

[37] H. Raether, "Surface plasmons on gratings," *Surface Plasmons on Smooth and Rough Surfaces and on Gratings*, pp. 91-116, 1988.

[38] P. Grant, S. Kaul, S. Chinnayelka, and M. McShane, "Fiber optic biosensors comprising nanocomposite multilayered polymer and nanoparticle ultrathin films," in *Engineering in Medicine and Biology Society, 2003. Proceedings of the 25th Annual International Conference of the IEEE*, 2003, pp. 2987-2990.

[39] B. Lee, S. Roh, and J. Park, "Current status of micro-and nano-structured optical fiber sensors," *Optical Fiber Technology*, vol. 15, pp. 209-221, 2009.

[40] J. Homola, *Surface plasmon resonance based sensors* vol. 4: Springer, 2006.

[41] S. Kim, H. Kim, Y. Lim, and B. Lee, "Off-axis directional beaming of optical field diffracted by a single subwavelength metal slit with asymmetric dielectric surface gratings," *Applied physics letters*, vol. 90, p. 051113, 2007.

[42] J. Homola, "Optical fiber sensor based on surface plasmon excitation," *Sensors and actuators B: chemical*, vol. 29, pp. 401-405, 1995.

[43] S. Al-Bader and M. Imtaar, "Azimuthally uniform surface-plasma modes in thin metallic cylindrical shells," *Quantum Electronics, IEEE Journal of,* vol. 28, pp. 525533, 1992.

[44] S. J. Al-Bader and M. Imtaar, "Optical fiber hybrid-surface plasmon polaritons," *JOSA B,* vol. 10, pp. 83-88, 1993.

[45] A. Díez, M. V. Andrés, and J. L. Cruz, "Hybrid surface plasma modes in circular metal-coated tapered fibers," *JOSA A,* vol. 16, pp. 2978-2982, 1999.

[46] A. K. Sharma and B. Gupta, "Influence of dopants on the performance of a fiber optic surface plasmon resonance sensor," *Optics communications,* vol. 274, pp. 320-326, 2007.

[47] M. Manuel, B. Vidal, R. López, S. Alegret, J. Alonso-Chamarro, I. Garces, and J. Mateo, "Determination of probable alcohol yield in musts by means of an SPR optical sensor," *Sensors and Actuators B: Chemical,* vol. 11, pp. 455-459, 1993.

[48] K. Matsubara, S. Kawata, and S. Minami, "Optical chemical sensor based on surface plasmon measurement," *Applied Optics,* vol. 27, pp. 1160-1163, 1988.

[49] B. Liedberg, I. Lundström, and E. Stenberg, "Principles of biosensing with an extended coupling matrix and surface plasmon resonance," *Sensors and Actuators B: Chemical,* vol. 11, pp. 63-72, 1993.

[50] L.-M. Zhang and D. Uttamchandani, "Optical chemical sensing employing surface plasmon resonance," *Electronics Letters,* vol. 24, pp. 1469-1470, 1988.

[51] R. Jorgenson and S. Yee, "A fiber-optic chemical sensor based on surface plasmon resonance," *Sensors and Actuators B: Chemical,* vol. 12, pp. 213-220, 1993.

[52] P. Vukusic, G. Bryan-Brown, and J. Sambles, "Surface plasmon resonance on gratings as a novel means for gas sensing," *Sensors and Actuators B: Chemical,* vol. 8, pp. 155-160, 1992.

[53] S. Nelson, K. S. Johnston, and S. S. Yee, "High sensitivity surface plasmon resonace sensor based on phase detection," *Sensors and Actuators B: Chemical,* vol. 35, pp. 187-191, 1996.

[54] P. Nikitin, A. Beloglazov, V. Kochergin, M. Valeiko, and T. Ksenevich, "Surface plasmon resonance interferometry for biological and chemical sensing," *Sensors and Actuators B: Chemical,* vol. 54, pp. 43-50, 1999.

[55] A. Kruchinin and Y. G. Vlasov, "Surface plasmon resonance monitoring by means of polarization state measurement in reflected light as the basis of a DNA-probe biosensor," *Sensors and Actuators B: Chemical,* vol. 30, pp. 77-80, 1996.

[56] B. Sepúlveda, A. Calle, L. M. Lechuga, and G. Armelles, "Highly sensitive detection of biomolecules with the magneto-optic surface-plasmon-resonance sensor," *Optics letters*, vol. 31, pp. 1085-1087, 2006.

[57] C. E. Jordan, A. G. Frutos, A. J. Thiel, and R. M. Corn, "Surface plasmon resonance imaging measurements of DNA hybridization adsorption and streptavidin/DNA multilayer formation at chemically modified gold surfaces," *Analytical Chemistry*, vol. 69, pp. 4939-4947, 1997.

[58] C. E. Jordan and R. M. Corn, "Surface plasmon resonance imaging measurements of electrostatic biopolymer adsorption onto chemically modified gold surfaces," *Analytical chemistry*, vol. 69, pp. 1449-1456, 1997.

[59] B. P. Nelson, A. G. Frutos, J. M. Brockman, and R. M. Corn, "Near-infrared surface plasmon resonance measurements of ultrathin films. 1. Angle shift and SPR imaging experiments," *Analytical chemistry*, vol. 71, pp. 3928-3934, 1999.

[60] B. P. Nelson, T. E. Grimsrud, M. R. Liles, R. M. Goodman, and R. M. Corn, "Surface plasmon resonance imaging measurements of DNA and RNA hybridization adsorption onto DNA microarrays," *Analytical chemistry*, vol. 73, pp. 1-7, 2001.

[61] E. Fu, J. Foley, and P. Yager, "Wavelength-tunable surface plasmon resonance microscope," *Review of scientific instruments*, vol. 74, pp. 3182-3184, 2003.

[62] A. W. Wark, H. J. Lee, and R. M. Corn, "Long-range surface plasmon resonance imaging for bioaffinity sensors," *Analytical chemistry*, vol. 77, pp. 3904-3907, 2005.

[63] A. Zybin, C. Grunwald, V. M. Mirsky, J. Kuhlmann, O. S. Wolfbeis, and K. Niemax, "Double-wavelength technique for surface plasmon resonance measurements: Basic concept and applications for single sensors and two-dimensional sensor arrays," *Analytical chemistry*, vol. 77, pp. 2393-2399, 2005.

[64] J. S. Shumaker-Parry, R. Aebersold, and C. T. Campbell, "Parallel, quantitative measurement of protein binding to a 120-element double-stranded DNA array in real time using surface plasmon resonance microscopy," *Analytical Chemistry*, vol. 76, pp. 2071-2082, 2004.

[65] J. S. Shumaker-Parry and C. T. Campbell, "Quantitative methods for spatially resolved adsorption/desorption measurements in real time by surface plasmon resonance microscopy," *Analytical chemistry*, vol. 76, pp. 907-917, 2004.

[66] C. T. Campbell and G. Kim, "SPR microscopy and its applications to high-throughput analyses of biomolecular binding events and their kinetics," *Biomaterials*, vol. 28, pp. 2380-2392, 2007.

[67] M. Piliarik, J. Katainen, and J. Homola, "Novel polarization control for highthroughput surface plasmon resonance sensors," in *Proceeding of SPIE*, 2007, p. 658515.

[68] M. Piliarik, H. Vaisocherová, and J. Homola, "A new surface plasmon resonance sensor for high-throughput screening applications," *Biosensors and Bioelectronics*, vol. 20, pp. 2104-2110, 2005.

[69] X. Guo, "Surface plasmon resonance based biosensor technique: A review," *Journal of biophotonics*, vol. 5, pp. 483-501, 2012.

[70] S. Löfås, M. Malmqvist, I. Rönnberg, E. Stenberg, B. Liedberg, and I. Lundström, "Bioanalysis with surface plasmon resonance," *Sensors and Actuators B: Chemical*, vol. 5, pp. 79-84, 1991.

[71] R. Karlsson and R. Stahlberg, "Surface plasmon resonance detection and multispot sensing for direct monitoring of interactions involving low-molecular-weight analytes and for determination of low affinities," *Analytical biochemistry*, vol. 228, pp. 274280, 1995.

[72] E. Nice and B. Catimel, "Instrumental biosensors: new perspectives for the analysis of biomolecular interactions," *Bioessays*, vol. 21, pp. 339-352, 1999.

[73] H. C. Pedersen, W. Zong, M. H. Sørensen, and C. Thirstrup, "Integrated holographic grating chip for surface plasmon resonance sensing," *Optical Engineering*, vol. 43, pp. 2505-2510, 2004.

[74] J. Homola, J. Dostalek, S. Chen, A. Rasooly, S. Jiang, and S. S. Yee, "Spectral surface plasmon resonance biosensor for detection of staphylococcal enterotoxin B in milk," *International journal of food microbiology*, vol. 75, pp. 61-69, 2002.

[75] G. G. Nenninger, M. Piliarik, and J. Homola, "Data analysis for optical sensors based on spectroscopy of surface plasmons," *Measurement Science and Technology*, vol. 13, p. 2038, 2002.

[76] J. Homola, H. B. Lu, G. G. Nenninger, J. Dostálek, and S. S. Yee, "A novel multichannel surface plasmon resonance biosensor," *Sensors and Actuators B: Chemical*, vol. 76, pp. 403-410, 2001.

[77] P. Nikitin, A. Grigorenko, A. Beloglazov, M. Valeiko, A. Savchuk, O. Savchuk, G. Steiner, C. Kuhne, A. Huebner, and R. Salzer, "Surface plasmon resonance interferometry for micro-array biosensing," *Sensors and Actuators A: Physical*, vol. 85, pp. 189-193, 2000.

[78] R. Naraoka and K. Kajikawa, "Phase detection of surface plasmon resonance using rotating analyzer method," *Sensors and Actuators B: Chemical,* vol. 107, pp. 952-956, 2005.

[79] H. Ho, W. Law, S. Wu, X. Liu, S. Wong, C. Lin, and S. Kong, "Phase-sensitive surface plasmon resonance biosensor using the photoelastic modulation technique," *Sensors and Actuators B: Chemical,* vol. 114, pp. 80-84, 2006.

[80] H. Ho, W. Law, S. Wu, C. Lin, and S. Kong, "Real-time optical biosensor based on differential phase measurement of surface plasmon resonance," *Biosensors and BIOELECTRONICS,* vol. 20, pp. 2177-2180, 2005.

[81] R. Kooyman, H. Kolkman, J. Van Gent, and J. Greve, "Surface plasmon resonance immunosensors: sensitivity considerations," *Analytica Chimica Acta,* vol. 213, pp. 3545, 1988.

[82] V. Thomsen, D. Schatzlein, and D. Mercuro, "Limits of detection in spectroscopy," *Spectroscopy,* vol. 18, pp. 112-114, 2003.

[83] H. E. de Bruijn, R. P. Kooyman, and J. Greve, "Choice of metal and wavelength for surface-plasmon resonance sensors: some considerations," *Applied optics,* vol. 31, pp. 440_1-442, 1992.

[84] E. M. Yeatman, "Resolution and sensitivity in surface plasmon microscopy and sensing," *Biosensors and Bioelectronics,* vol. 11, pp. 635-649, 1996.

[85] J. Homola, I. Koudela, and S. S. Yee, "Surface plasmon resonance sensors based on diffraction gratings and prism couplers: sensitivity comparison," *Sensors and Actuators B: Chemical,* vol. 54, pp. 16-24, 1999.

[86] J. Homola, "On the sensitivity of surface plasmon resonance sensors with spectral interrogation," *Sensors and Actuators B: Chemical,* vol. 41, pp. 207-211, 1997.

[87] A. A. Kolomenskii, P. Gershon, and H. Schuessler, "Sensitivity and detection limit of concentration and adsorption measurements by laser-induced surface-plasmon resonance," *Applied optics,* vol. 36, pp. 6539-6547, 1997.

[88] T. M. Chinowsky, L. S. Jung, and S. S. Yee, "Optimal linear data analysis for surface plasmon resonance biosensors," *Sensors and Actuators B: Chemical,* vol. 54, pp. 8997, 1999.

[89] A. K. Sharma and B. Gupta, "Comparison of performance parameters of conventional and nano-plasmonic fiber optic sensors," *Plasmonics,* vol. 2, pp. 51-54, 2007.

[90] Y. S. Dwivedi, A. K. Sharma, and B. Gupta, "Influence of design parameters on the performance of a surface plasmon sensor based fiber optic sensor," *Plasmonics*, vol. 3, pp. 79-86, 2008.

[91] C. Ronot-Trioli, A. Trouillet, C. Veillas, and H. Gagnaire, "Monochromatic excitation of surface plasmon resonance in an optical-fibre refractive-index sensor," *Sensors and Actuators A: Physical*, vol. 54, pp. 589-593, 1996.

[92] R. K. Verma, A. K. Sharma, and B. Gupta, "Surface plasmon resonance based tapered fiber optic sensor with different taper profiles," *Optics Communications*, vol. 281, pp. 1486-1491, 2008.

[93] D. Monzón-Hernández and J. Villatoro, "High-resolution refractive index sensing by means of a multiple-peak surface plasmon resonance optical fiber sensor," *Sensors and Actuators B: Chemical*, vol. 115, pp. 227-231, 2006.

[94] S.-F. Wang, M.-H. Chiu, J.-C. Hsu, R.-S. Chang, and F.-T. Wang, "Theoretical analysis and experimental evaluation of D-type optical fiber sensor with a thin gold film," *Optics communications*, vol. 253, pp. 283-289, 2005.

[95] M.-H. Chiu, C.-H. Shih, and M.-H. Chi, "Optimum sensitivity of single-mode D-type optical fiber sensor in the intensity measurement," *Sensors and Actuators B: Chemical*, vol. 123, pp. 1120-1124, 2007.

[96] M. Piliarik, J. Homola, Z. Manıková, and J. Čtyroký, "Surface plasmon resonance sensor based on a single-mode polarization-maintaining optical fiber," *Sensors and Actuators B: Chemical*, vol. 90, pp. 236-242, 2003.

[97] H. Suzuki, M. Sugimoto, Y. Matsui, and J. Kondoh, "Effects of gold film thickness on spectrum profile and sensitivity of a multimode-optical-fiber SPR sensor," *Sensors and Actuators B: Chemical*, vol. 132, pp. 26-33, 2008.

[98] Y.-J. Chang, Y.-C. Chen, H.-L. Kuo, and P.-K. Wei, "Nanofiber optic sensor based on the excitation of surface plasmon wave near fiber tip," *Journal of biomedical optics*, vol. 11, pp. 14032-14032, 2006.

[99] F. Villuendas and J. Pelayo, "Optical fibre device for chemical seming based on surface plasmon excitridon," *Sensors and Actuators A: Physical*, vol. 23, pp. 11421145, 1990.

[100] I. Garces, C. Aldea, and J. Mateo, "Four-layer chemical fibre optic plasmon-based sensor," *Sensors and Actuators B: Chemical*, vol. 7, pp. 771-774, 1992.

[101] L. De Maria, M. Martinelli, and G. Vegetti, "Fiber-optic sensor based on surface plasmon interrogation," *Sensors and Actuators B: Chemical*, vol. 12, pp. 221-223, 1993.

[102] M. Mar, R. Jorgenson, S. Letellier, and S. Yee, "In-situ characterization of multilayered Langmuir-Blodgett films using a surface plasmon resonance fiber optic sensor," in *Engineering in Medicine and Biology Society, 1993. Proceedings of the 15th Annual International Conference of the IEEE*, 1993, pp. 1551-1552.

[103] R. C. Jorgenson and S. S. Yee, "Control of the dynamic range and sensitivity of a surface plasmon resonance based fiber optic sensor," *Sensors and Actuators A: Physical*, vol. 43, pp. 44-48, 1994.

[104] M. Niggemann, A. Katerkamp, M. Pellmann, P. Bolsmann, J. Reinbold, and K. Cammann, "Remote sensing of tetrachloroethene with a micro-fibre optical gas sensor based on surface plasmon resonance spectroscopy," *Sensors and Actuators B: Chemical*, vol. 34, pp. 328-333, 1996.

[105] R. Slavık, J. Homola, J. Čtyroký, and . Brynda, "Novel spectral fiber optic sensor based on surface plasmon resonance," *Sensors and Actuators B: Chemical*, vol. 74, pp. 106-111, 2001.

[106] A. Abdelghani, J. Chovelon, N. Jaffrezic-Renault, C. Ronot-Trioli, C. Veillas, and H. Gagnaire, "Surface plasmon resonance fibre-optic sensor for gas detection," *Sensors and Actuators B: Chemical*, vol. 39, pp. 407-410, 1997.

[107] A. Dıez, M. Andrés, and J. Cruz, "In-line fiber-optic sensors based on the excitation of surface plasma modes in metal-coated tapered fibers," *Sensors and Actuators B: Chemical*, vol. 73, pp. 95-99, 2001.

[108] W. B. Lin, M. Lacroix, J. M. Chovelon, N. Jaffrezic-Renault, and H. Gagnaire, "Development of a fiber-optic sensor based on surface plasmon resonance on silver film for monitoring aqueous media," *Sensors and Actuators B: Chemical*, vol. 75, pp. 203-209, 2001.

[109] Ó. Esteban, R. Alonso, M. Navarrete, and A. Gonzàlez-Cano, "Surface plasmon excitation in fiber-optics sensors: A novel theoretical approach," *Journal of lightwave technology*, vol. 20, p. 448, 2002.

[110] Y.-J. He, Y.-L. Lo, and J.-F. Huang, "Optical-fiber surface-plasmon-resonance sensor employing long-period fiber gratings in multiplexing," *JOSA B*, vol. 23, pp. 801-811, 2006.

[111] J.-L. Tang, S.-F. Cheng, W.-T. Hsu, T.-Y. Chiang, and L.-K. Chau, "Fiber-optic biochemical sensing with a colloidal gold-modified long period fiber grating," *Sensors and Actuators B: Chemical*, vol. 119, pp. 105-109, 2006.

[112] G. Nemova and R. Kashyap, "Fiber-Bragg-grating-assisted surface plasmon-polariton sensor," *Optics letters,* vol. 31, pp. 2118-2120, 2006.

[113] G. Nemova and R. Kashyap, "Modeling of plasmon-polariton refractive-index hollow core fiber sensors assisted by a fiber Bragg grating," *Lightwave Technology, Journal of,* vol. 24, pp. 3789-3796, 2006.

[114] T. Allsop, R. Neal, S. Rehman, D. J. Webb, D. Mapps, and I. Bennion, "Characterization of infrared surface plasmon resonances generated from a fiberoptical sensor utilizing tilted Bragg gratings," *JOSA B,* vol. 25, pp. 481-490, 2008.

[115] W. Ding, S. Andrews, T. Birks, and S. Maier, "Modal coupling in fiber tapers decorated with metallic surface gratings," *Optics letters,* vol. 31, pp. 2556-2558, 2006.

[116] A. Hassani, B. Gauvreau, M. F. Fehri, A. Kabashin, and M. Skorobogatiy, "Photonic crystal fiber and waveguide-based surface plasmon resonance sensors for application in the visible and near-IR," *Electromagnetics,* vol. 28, pp. 198-213, 2008.

[117] A. Hassani and M. Skorobogatiy, "Design criteria for microstructured-optical-fiberbased surface-plasmon-resonance sensors," *JOSA B,* vol. 24, pp. 1423-1429, 2007.

[118] M. Hautakorpi, M. Mattinen, and H. Ludvigsen, "Surface-plasmon-resonance sensor based on three-hole microstructured optical fiber," *Optics express,* vol. 16, pp. 84278432, 2008.

[119] W. Qin, S. Li, Y. Yao, X. Xin, and J. Xue, "Analyte-filled core self-calibration microstructured optical fiber based plasmonic sensor for detecting high refractive index aqueous analyte," *Optics and Lasers in Engineering,* vol. 58, pp. 1-8, 2014.

[120] J. N. Dash and R. Jha, "SPR Biosensor Based on Polymer PCF Coated With Conducting Metal Oxide," *IEEE Photonics Technology Letters,* vol. 26, pp. 595-598, 2014.

[121] S. A. Cerqueira Jr, "Recent progress and novel applications of photonic crystal fibers," *Reports on progress in physics,* vol. 73, p. 024401, 2010.

[122] V. Kumar, A. George, W. Reeves, J. Knight, P. Russell, F. Omenetto, and A. Taylor, "Extruded soft glass photonic crystal fiber for ultrabroad supercontinuum generation," *Optics Express,* vol. 10, pp. 1520-1525, 2002.

[123] X. Feng, A. K. Mairaj, D. W. Hewak, and T. M. Monro, "Towards high-index glass based monomode holey fibre with large mode area," *Electronics Letters,* vol. 40, pp. 167-169, 2004.

[124] A. Mori, K. Shikano, K. Enbutsu, K. Oikawa, K. Naganuma, M. Kato, and S. Aozasa, "1.5 μm band zero-dispersion shifted tellurite photonic crystal fibre with a nonlinear

coefficient γ of 675 W− 1km− 1," in *Eur. Conf. Opt. Commun.(ECOC), Stockholm, Sweden*, 2004.

[125] E. Akowuah, T. Gorman, S. Haxha, and J. Oliver, "Dual channel planar waveguide surface plasmon resonance biosensor for an aqueous environment," *Optics express*, vol. 18, pp. 24412-24422, 2010.

[126] J. Hastings, J. Guo, P. Keathley, P. Kumaresh, Y. Wei, S. Law, and L. Bachas, "Optimal self-referenced sensing using long-and short-range surface plasmons," *Optics express*, vol. 15, pp. 17661-17672, 2007.

[127] R. Slavík and J. Homola, "Simultaneous excitation of long and short range surface plasmons in an asymmetric structure," *Optics communications*, vol. 259, pp. 507-512, 2006.

[128] J. Burke, G. Stegeman, and T. Tamir, "Surface-polariton-like waves guided by thin, lossy metal films," *Physical Review B*, vol. 33, p. 5186, 1986.

[129] J. Guo, "Multi-mode Self-referencing Surface Plasmon Resonance Sensors," 2013.

[130] S. Guo, F. Wu, S. Albin, H. Tai, and R. Rogowski, "Loss and dispersion analysis of microstructured fibers by finite-difference method," *Optics Express*, vol. 12, pp. 3341-3352, 2004.

[131] S. Obayya, B. Rahman, and K. Grattan, "Accurate finite element modal solution of photonic crystal fibres," *IEE Proceedings-Optoelectronics*, vol. 152, pp. 241-246, 2005.

[132] K. Saitoh and M. Koshiba, "Full-vectorial finite element beam propagation method with perfectly matched layers for anisotropic optical waveguides," *Journal of lightwave technology*, vol. 19, p. 405, 2001.

[133] D. Ferrarini, L. Vincetti, M. Zoboli, A. Cucinotta, and S. Selleri, "Leakage properties of photonic crystal fibers," *Optics Express*, vol. 10, pp. 1314-1319, 2002.

[134] J. D. Joannopoulos, R. D. Meade, and J. Winn, "Photonic crystals: molding the flow of light, 1995," *Appendix D, PRINCETON*, 1997.

[135] A. Cucinotta, S. Selleri, L. Vincetti, and M. Zoboli, "Holey fiber analysis through the finite-element method," *Photonics Technology Letters, IEEE*, vol. 14, pp. 1530-1532, 2002.

[136] S. Obayya, B. Rahman, and H. El-Mikati, "New full-vectorial numerically efficient propagation algorithm based on the finite element method," *Journal of lightwave technology*, vol. 18, p. 409, 2000.

[137] R. P. C. GmbH, "Effective Refractive Index," 2014.

[138] F. Zolla, G. Renversez, A. Nicolet, B. Kuhlmey, S. Guenneau, D. Felbacq, A. Argyros, and S. Leon-Saval, *Foundations of photonic crystal fibres*: World Scientific, 2005.

[139] W. Sellmeier, "Zur erklärung der abnormen farbenfolge im spectrum einiger substanzen," *Annalen der Physik und Chemie,* vol. 219, pp. 272-282, 1871.

[140] R. Otupiri, E. Akowuah, S. Haxha, H. Ademgil, F. AbdelMalek, and A. Aggoun, "A Novel birefrigent photonic crystal fibre surface plasmon resonance biosensor," *Photonics Journal, IEEE,* vol. 6, 2014.

[141] M. INC, "MATLAB - The Language of Technical Computing - B."

[142] E. K. Akowuah, T. Gorman, H. Ademgil, S. Haxha, G. K. Robinson, and J. V. Oliver, "Numerical analysis of a photonic crystal fiber for biosensing applications," *Quantum Electronics, IEEE Journal of,* vol. 48, pp. 1403-1410, 2012.

[143] M. Piliarik, L. Párová, and J. Homola, "High-throughput SPR sensor for food safety," *Biosensors and Bioelectronics,* vol. 24, pp. 1399-1404, 2009.

[144] J. A. Harrington, "A review of IR transmitting, hollow waveguides," *Fiber & Integrated Optics,* vol. 19, pp. 211-227, 2000.

[145] P. Falkenstein and B. L. Justus, "Fused array preform fabrication of holey optical fibers," ed: Google Patents, 2013.

[146] X. Yu, Y. Zhang, S. Pan, P. Shum, M. Yan, Y. Leviatan, and C. Li, "A selectively coated photonic crystal fiber based surface plasmon resonance sensor," *Journal of Optics,* vol. 12, p. 015005, 2010.

[147] B. T. Kuhlmey, B. J. Eggleton, and D. K. Wu, "Fluid-filled solid-core photonic bandgap fibers," *Journal of Lightwave Technology,* vol. 27, pp. 1617-1630, 2009.

[148] K. Nielsen, D. Noordegraaf, T. Sørensen, A. Bjarklev, and T. P. Hansen, "Selective filling of photonic crystal fibres," *Journal of Optics A: Pure and Applied Optics,* vol. 7, p. L13, 2005.

[149] N. Takeyasu, T. Tanaka, and S. Kawata, "Metal deposition deep into microstructure by electroless plating," *Japanese journal of applied physics,* vol. 44, p. L1134, 2005.

[150] P. J. Sazio, A. Amezcua-Correa, C. E. Finlayson, J. R. Hayes, T. J. Scheidemantel, N. F. Baril, B. R. Jackson, D.-J. Won, F. Zhang, and E. R. Margine, "Microstructured optical fibers as high-pressure microfluidic reactors," *Science,* vol. 311, pp. 15831586, 2006.

Appendix A

List of Publications

1. Otupiri, R., Akowuah, E., Haxha, S., Ademgil, H., AbdelMalek, F., Aggoun, A. A Novel birefrigent photonic crystal fibre surface plasmon resonance bio sensor. 2014

Appendix B

MATLAB Scripts

Confinement loss Calculation

```
%  Author: Robert Otupiri, 2014
%  Confinment Loss Calculation
clear clc
lamda = xlsread('sample.xlsx','lamda');% Load wave length values imag
=  xlsread('sample.xlsx','conloss_HEx_HEy_tau40');%Load imaginary
refractive index values

lamdaa = lamda(:,1); %Lamda in nm plotin_lamd
= lamda(:,2) ; %Lamda in um

k=(2*pi)./lamdaa;% Calculate the variable k in the confinement loss
equation

HEx = imag(:,1:3);%Define imaginary refractive index values of x polarised
fundamental mode
HEy = imag(:,4:6);%Define imaginary refractive index values of y polarised
fundamental mode



L = size(HEx) col
= L(:,2)



for a=1:col;
HEx_losses(:,a)=(8.686*k .* HEx(:,a)) ./ 100;%Confinement loss for x
polarised fundamental

HEy_losses(:,a)=(8.686*k .* HEy(:,a)) ./ 100;%%Confinement loss for y
polarised fundamental

end
yHEx = HEx_losses; yHEy
= HEy_losses;
```

```
  w_length =
lamda(:,2)  x =
w_length;


col = size(yHEx);%the columns of the transmission parameters  count = 1;
x_values = ones(1,2);  for z = 1:col(1,2)      count = 1;    clear
x_values      x_values = ones(1,2);  fittmex =
fit(w_length,yHEx(:,z),'smoothingspline');%curve fitting for x polarised
fundamental
fittmey = fit(w_length,yHEy(:,z),'smoothingspline');%curve fitting for y
polarised fundamental
  new_x = 550:1:950;  new_x =
new_x';  new_yHEx(:,z) =
fittmex(new_x);  new_yHEy(:,z)
= fittmey(new_x);
  end
subplot(1,2,1)
plot(new_x,new_yHEx)
subplot(1,2,2)
plot(new_x,new_yHEy)
```

Dispersison Plot Script

```
%  Author: Robert Otupiri, 2014
%  Dispersion plot script
  clear
clc
lamda = xlsread('sample.xlsx','lamda');%Load wave length values
real_neff = xlsread('sample.xlsx','conloss_HEx_HEy_tau40');%Load real
refractive index values
y = real_neff;% Re-assign real refractive index values  w_length
= lamda(:,2);%Re-assign

%new_y = y;%will fill this up with the new data dont mind my programming
efficiency. It gets the work done that is all!  col = size(y);%the
columns of the transmission parameters  ount = 1;  x_values = ones(1,2);
for z = 1:col(1,2)      count = 1;    clear x_values      x_values =
ones(1,2);  fittme = fit(w_length,y(:,z),'poly1');%curve fitting for x
polarised fundamental
new_x = 500:1000;%Redefine range of wavelength  new_x = new_x';
new_y(:,z) = fittme(new_x);%Associating redefined x values with y values

end
plot(new_x,new_y)
```

Amplitude Sensitivity Calculation Script

```
%  Author: Robert Otupiri, 2014
%  Amplitude sensitivity  script
```

```
%this function will draw the plasma curve for any given data from pcf
clc clear
%load the x and y values %load
w_length.txt
y_all = xlsread('5loss spectra for variation of gold
thickness.xlsx','HEy_loss_value_to_calc_ampsens');
  y = y_all; w_length = y_all(:,1);%extract the
wavelength component


%new_y = y;%will fill this up with the new data dont mind my programming
efficiency. It gets the work done that is all! col = size(y);%the
columns of the transmission parameters k = length (y); count = 1;
x_values = ones(1,2);
S_amp = ones(k,col(1,2))%amplitude sensitivity

lambda_ = w_length;
%we are going to compute the losses for
i = 1:k
  S_amp (i,1)= -1*(((y(i,2)-y(i,3))/0.01)/y(i,3));%find the amplitude
sensitivity according to hassani et al
  S_amp (i,2)= -1*(((y(i,4)-y(i,5))/0.01)/y(i,5));%find the amplitude
sensitivity according to hassani et al
  S_amp (i,3)= -1*(((y(i,6)-y(i,7))/0.01)/y(i,7));%find the amplitude
sensitivity according to hassani et al

end


Results = [w_length, S_amp];
    y = S_amp;
%y = yy_175(:,1);

x = w_length;

%new_y = y;%will fill this up with the new data dont mind my programming
efficiency. It gets the work done that is all! col = size(y);%the
columns of the transmission parameters tol = 1e-3;%not needed anymore
count = 1;
x_values = ones(1,2); % perform a fit to the
function for z = 1:col(1,2)     count = 1;
clear x_values     x_values = ones(1,2); fittme
= fit(w_length,y(:,z),'smoothingspline');

new_x = 500:1:1000; new_x
= new_x'; new_y(:,z) =
fittme(new_x);

end
plot(new_x,new_y)
```